Ordered mesoporous carbons obtained from low-value coal tar products for electrochemical energy storage and water remediation

Alberto Castro-Muñiz, Sara Lorenzo-Fierro, Amelia Martinez-Alonso, Juan M.D. Tascon, Vanessa Fierro, Fabián Suárez-García, Juan Paredes

Highlights

- Creosote, a low-priced coal tar distillation product, was used as carbon precursor
- Simple one step infiltration in acidic medium at moderate temperature was optimized
- The obtained ordered mesoporous carbons had a very well-developed mesopore network
- The materials showed good performance as supercapacitors and dye adsorbents

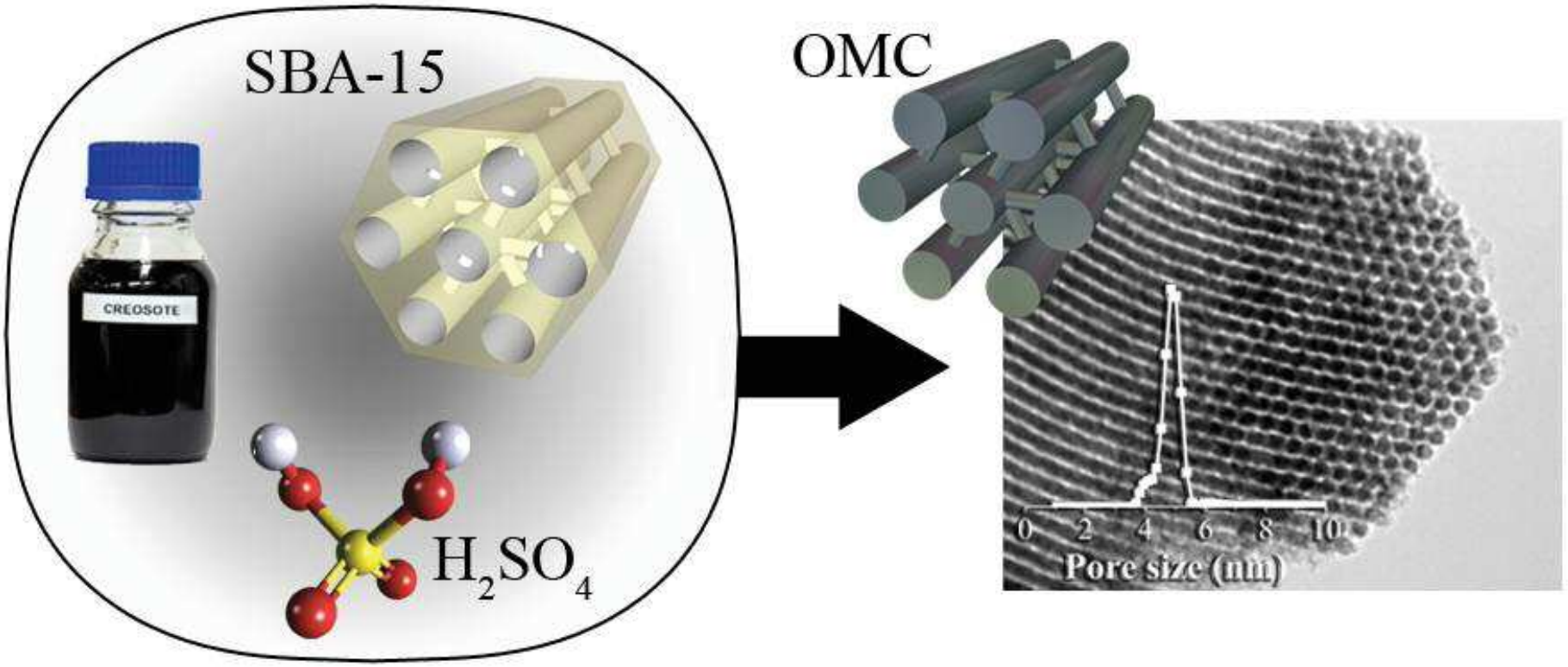
SBA-15
CREOSOTE
H_2SO_4
OMC
0 2 4 6 8 10
Pore size (nm)

Ordered mesoporous carbons obtained from low-value coal tar products for electrochemical energy storage and water remediation

Alberto Castro-Muñiz[1]*, Sara Lorenzo-Fierro[1], Amelia Martínez-Alonso[1], Juan M.D. Tascón[1], Vanessa Fierro[2], Fabián Suárez-García[1], Juan I. Paredes[1].

[1] Instituto Nacional del Carbón (INCAR-CSIC), C/Francisco Pintado Fe 26, 33011, Oviedo, Spain.
[2] Institute Jean Lamour, UMR CNRS, University of Lorraine, ENSTIB, 27 Rue Philippe Séguin, BP 21042, 88051.

* Corresponding Author: alberto@incar.csic.es

Abstract

Ordered mesoporous carbons (OMCs) obtained by the hard-templating method are usually prepared using complicated infiltration procedures and/or relatively high-priced carbon precursors. In this work, OMCs were obtained using creosote, a modestly priced substance obtained from the distillation of coal tar, as a carbon precursor and an ordered mesoporous silica (SBA-15) as the template. The porous network of the template was infiltrated using a simple, one-step method in acidic medium at a moderate temperature, making it potentially scalable for mass production. Optimization of the synthesis conditions led to OMCs with a very well ordered porosity with a very narrow pore size distribution in the mesopore region, together with a high surface area. This material was tested as an electrode for electrochemical energy storage devices and as an adsorbent for pollutant removal. Owing to its well-developed hierarchical pore network, the present OMC showed a good performance as a supercapacitor electrode in aqueous electrolyte and high rate of methylene blue dye adsorption.

Keywords: Ordered Mesoporous Carbons; Hard template; Coal-tar products; Electrochemical Energy Storage; Dye Removal.

Highlights

- Creosote, a low-priced coal tar distillation product, was used as carbon precursor
- Simple one step infiltration in acidic medium at moderate temperature was optimized
- The obtained ordered mesoporous carbons had a very well-developed mesopore network
- The materials showed good performance as supercapacitors and dye adsorbents

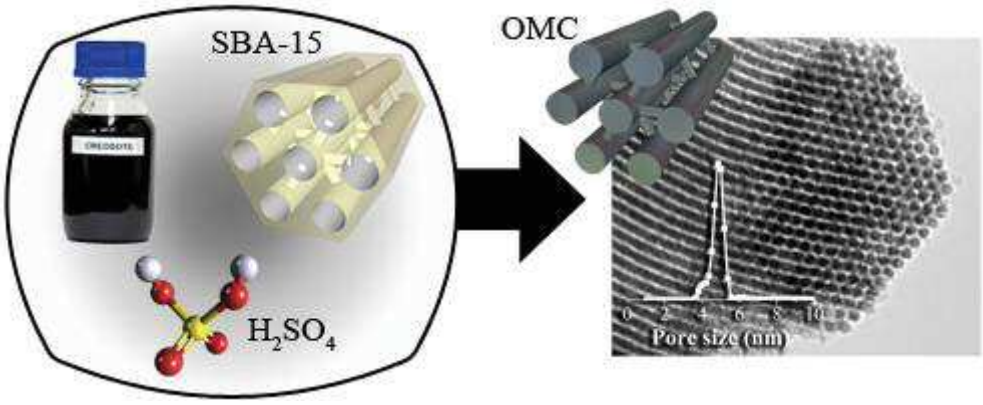

1 Introduction

Conventional porous carbon materials are obtained from carbon-rich precursors such as lignocellulosic residues or mineral coal. After the carbonization of the precursor material, the product is submitted to an activation process to further develop the porosity of the final activated carbon. Control over the activation conditions allows tuning the porous texture [1]. However, high-demanding applications (*e.g.*, energy storage, electrocatalysis or water remediation) require materials with a very fine tuned porosity, especially in the mesopore range (2-50 nm in size).

Different techniques have been developed to approach this problem. Amongst them, the hard-templating method stands out as a powerful strategy for creating carbon materials with strictly controlled porosity, including ordered mesoporous carbons (OMCs). The templated carbon materials are synthesized by the infiltration of a carbon precursor into the pore network of an inorganic porous solid that acts as a template [2–4]. After the infiltration of the precursor, the mixture is carbonized and then the template is removed by an appropriate etching procedure. Thus, a carbonaceous material is obtained with a porous structure that is a replica of the walls of the material used as a template. By using different templates, the main pore size and the pore morphology can be accurately controlled. In the case of OMCs, the usual choice as a template are mesoporous oxides like silica. However, the success in replicating the template depends largely on the stringent control of a number of factors. A key point is the selection of a suitable carbon precursor, which must infiltrate the template homogeneously, polymerize and afford a high carbon yield after pyrolysis. Frequently used precursors are sucrose, furfuryl alcohol, acrylonitrile, phenol resin, propylene, acetylene or acetonitrile, among others [5].

Polycyclic aromatic hydrocarbons have been used as carbon precursors for the preparation of hierarchical porous carbons [6–11]. These materials have been used also to infiltrate the templates in the hard-templating method [12]. The OMCs obtained using these carbon precursors exhibit better electrical conductivity than that of porous carbons obtained using more conventional carbon precursors because of the higher aromatic character of the former [13,14]. However, a comparatively small number of studies have focused on the preparation of OMCs using these carbon precursors. Acenaphthene has been employed as a precursor with Al-modified MCM-48, SBA-1, SBA-15 and KIT-6 silicas as templates for the synthesis of OMCs in an autoclave at high temperature and high pressure [14,15]. Milder synthesis procedures are a priori more attractive and have made use of naphthalene, anthracene, or pyrene dissolved in acetone as a carbon precursor and SBA-15 [12] or MSU-H [16] as a template with sulfuric acid to act as a polymerization catalyst at room temperature. A similar method has been followed to infiltrate MSU-H with phenanthrene dissolved in acetone, but using toluene sulfonic acid as a catalyst [17,18]. Anthracene has also been introduced in the pores of MCM-41 by dissolving it in dichloromethane [19]. More recently, only two studies have focused on the preparation of OMCs using polycyclic aromatic compounds. Both of them used phenanthroline dissolved in ethanol, in the presence of $FeCl_2$ [20] and H_2SO_4 [21] as

catalysts, and SBA-15 and mesoporous silica spheres as templates, respectively. All these previous studies made use of pure , relatively expensive polyaromatic compounds, which are solid at ambient temperature, so the infiltration of the templates must be either carried out in an autoclave at high temperatures and pressures or by dissolving the carbon precursors in a solvent (*e.g.*, acetone), thus making the process less amenable to industrial upscaling. For example, the use of a solvent requires the repetition of the impregnation step several times to achieve a complete filling of the template pores, and the evaporation of the solvent after each step impedes an optimum impregnation.

To circumvent this issue, in the present work we have made use of creosote as a carbon precursor for the preparation of OMCs by the hard-template method. Creosote is a low-priced product obtained through distillation of coal tar in the temperature range between 240 and 350 °C, and is made up of a complex mixture of polycyclic aromatic hydrocarbons, its main components being phenanthrene, acenaphthene, naphthalene, fluorene and dibenzofuran, which collectively amount to ~50% of its total weight. Creosotes are typically employed as wood preservatives and, to the best of our knowledge, they have never been used as a precursor for the synthesis of any type of carbon material (including OMCs). Creosotes are generally liquid at room temperature or close to room temperature. This feature would avoid the need to use high temperatures or solvents when infiltrating the creosotes into hard templates, making them more convenient precursors in the synthesis of OMCs compared to pure, single-component polycyclic aromatic hydrocarbons. We demonstrate here that high quality OMCs can be efficiently prepared using such low-value, multi-component substance as the precursor, and the resulting carbons are competitive materials when used in electrochemical energy storage and water remediation applications.

2 Materials and methods

2.1 OMC preparation

The OMCs were prepared following the hard template method as schematically depicted in Figure SI 1 (Supporting Information). First, the pores of the template were infiltrated with the carbon precursor (creosote). Then, the infiltrated template was heat-treated to obtain a composite of the template with the carbon material. Finally, the template was removed by chemical etching to give a stand-alone carbon material.

2.1.1 Template synthesis

The template used in this work was the ordered mesoporous silica (OMS) SBA-15, which was prepared as follows [22]. First, 18.2 g of the non-ionic triblock copolymer surfactant Pluronic P123 was dissolved in 477.75 ml of distilled water with 91.00 ml of HCl (37 wt.%) by stirring the mixture for 24 h at 40 °C. Then, 40.57 ml of tetraethoxysilane (TEOS) were added and the mixture was further stirred for 4 h to allow the hydrolysis of the TEOS to take place. The solution was transferred to a 750 ml autoclave to age the silica precursor material at 110 °C for 72 h. The mixture was subsequently filtered, thoroughly washed with both distilled water and ethanol, and

dried at 80 °C overnight. Finally, the surfactant was removed by calcination at 550 °C for 6 h.

2.1.2 Carbon precursor

The carbon precursor used in this work was a creosote oil (supplied by the company Bilbaína de Alquitranes S.A., Spain), a low-value product obtained during the distillation of coal tar. Creosote consists of a complex mixture of aromatic compounds (see Table SI 1 in Supporting Information), with phenanthrene, acenaphthene, naphthalene, fluorene and dibenzofuran as its main components. The crystallization temperature of creosote used is 18.5 °C, so it is liquid at room temperature. However, the occurrence of crystals at the crystallization temperature could cause changes in the creosote composition, so working at temperatures above the crystallization temperature was necessary in order to avoid any variation in the chemical composition when an aliquot was taken from the original vessel. In addition, as will be discussed below, the creosote was polymerized by mixing it with H_2SO_4 at different volume ratios to promote the retention of carbon product in the silica template after the heat treatment.

2.1.3 Template infiltration

The SBA-15 was infiltrated with the carbon precursor following the method described in the scheme represented in Figure SI 2 in Supporting Information. First, 4.5 g of the OMS were degassed at 110 °C under vacuum overnight. Then, the temperature was decreased to the infiltration temperature, which was set to 40 °C to make sure that the creosote was completely liquid and its components were well mixed. The reactor was filled with argon, and the carbon precursor was put into contact with the OMS under stirring. The volume of the carbon precursor introduced in the reactor was calculated as 125 vol.% of the total pore volume of the OMS, obtained by N_2 adsorption. The mixture was kept under vigorous stirring while the reactor was vacuumed for 30 min. Then, the reactor was pressurized with argon. The pressure was kept slightly above atmospheric pressure for 30 min. This vacuum/pressure cycling was repeated until a homogenous mixture was observed (usually 3-4 times). Finally, the sample was heated up to 110 °C under argon pressure for 2 h. This procedure is similar to the one used industrially for the protection of wood by impregnation with creosote [23–25].

2.1.4 Ordered mesoporous carbons

The OMS/carbon precursor composite was carbonized in a horizontal furnace at 950 °C under an argon flow (heating rate: 1 °C/min; flow rate: 500 ml/min) to obtain a composite of OMS and carbon material. The carbon material was released from the template by washing the composite with 1 M NaOH solution at 40 °C for 24 h. The effectiveness of the washing was assessed by thermogravimetry and the NaOH was seen to be quite effective in dissolving the silica; less than 3 wt.% of SiO_2 remained. This procedure allowed us to circumvent the use of strong acids such as HF, which gave similar residual silica contents after the washing.

2.2 Characterization of materials

The amount of material infiltrated in the silica template was estimated in a thermobalance (SDT Q600 from TA) from the weight loss after the combustion of the sample in air at 850 °C for 1 h. The composition of the creosote and the H_2SO_4-treated creosote were analyzed using an Agilent Technologies Model 7890N gas chromatograph coupled to a mass selective detector 5975C and equipped with an autosampler 7693A. Separations were carried out on a fused-silica capillary column (25 m length x 0.22 mm i.d.) coated with HP-5MS stationary phase. The furnace temperature was increased at a heating rate of 4 °C/min from 50 to 325 °C keeping this temperature for 10 min. Identification was carried out by comparing their mass spectra with those found in spectral libraries or by performing a complete study of their fragmentation patterns. The microscopic morphology of the samples was studied by field emission scanning electron microscopy (FE-SEM; Quanta FEG 650 microscope, from FEI, at 25 kV). The nanometer-scale morphology and structure of the materials were analyzed with transmission electron microscopy (TEM; 2000 EX-II from JEOL, at 160 kV), and X-ray diffraction (XRD; D5000 diffractometer from Siemens), and Raman spectroscopy (LabRaman from Horiba Jobin Yvon), respectively. The porous texture of the materials was analyzed by physical adsorption of N_2 at -196 °C in a volumetric analyzer (Autosorb-1 from Quantachrome). The samples were degassed at 150 °C under vacuum overnight prior to the measurements. The BET surface area, S_{BET}, was calculated by the BET equation from the data in the relative pressure range of ca. 0.01 ~ 0.2 and the total pore volume, V_T, was obtained by the Gurvitsch rule from the amount of adsorbed N_2 at a relative pressure of 0.97 [26]. The micropore volume, $V_{\mu p,DR}$, was calculated by applying the Dubinin-Radushkevich method to the adsorption isotherms [26], and the mesopore volume, V_{mp}, was estimated as $V_{mp}=V_T - V_{\mu p,DR}$. The pore size distribution (PSD) of the samples was calculated by applying the non-local density functional theory (NLDFT) in the quenched solid density functional theory (QSDFT) method developed by Quantachrome [27] to the N_2 adsorption branch using the QSDFT equilibrium model, from which the main pore size, d_{DFT}, was obtained.

2.3 Performance evaluation of the materials in electrochemical energy storage and water remediation

2.3.1 Electrochemical energy storage (supercapacitors)

The materials were tested as electrodes for supercapacitors, which were prepared as a paste by mixing the active material with a conductive additive (carbon black, CB, Vulcan XC72R from Cabot Corp.) and a binder (polytetrafluoroethylene, PTFE, Sigma Aldrich), in a weight proportion of sample : CB : PTFE = 85 : 5 : 10. A circular sheet (10 mm in diameter) was prepared from the paste and pressed at 1000 kg for 1 min. The electrodes (~8 mg), were tested in aqueous electrolyte (1M H_2SO_4) using a Swagelok-type cell in 2- and 3-electrode cell configurations. In the 3-electrode cell, the reference electrode was Ag/AgCl [3M KCl-saturated AgCl (REF321 electrode from Hach)]. The counter electrodes were prepared in the same manner as described above but using a total mass of *ca.* 10 mg made up of a commercial activated carbon fiber (FR-20 from

Kuraray Co., Ltd.) as the active component. A cellulose separator (Whatman) was sandwiched between the working and counter electrodes. In the case of the 2-electrode cell, two electrodes prepared from the OMC samples with the same mass were used. The ensembles were soaked in the electrolyte for at least 48 h before the electrochemical measurements. Impedance spectroscopy within a frequency range of 10^{-2} ~ 10^{5} Hz, cyclic voltammetry (CV) (potential window 3-electrode cell: -0.1 ~ 0.8 V vs. Ag/AgCl: 2 electrode cell: 0-1 V), and galvanostatic charge/discharge cycling tests were carried out in a potentiostat (Biologic VSP). The specific values were obtained referred to the mass of the active material in the working electrode for the 3-electrode cell configuration and in both electrodes in the case of the 2-electrode cell. A commercial activated carbon (YP-50F from Kuraray Co., Ltd.) was also tested for comparison.

2.3.2 Water remediation (dye adsorption)

The carbon materials were tested as adsorbents for removing methylene blue (MB) from water. For the sake of comparison, three commercial activated carbons typically used for water treatment (S300, S1030 and P835, from Silcarbon Aktivkohle GmbH) were also tested. The maximum MB adsorption capacity, q_{MB}, of the samples was obtained by soaking 10 mg of the sample in 10 ml of MB solution (2 g/l) solution at 25 °C for 48 h. The adsorption kinetics of MB was determined by soaking 10 mg of the samples in 10 ml of a MB solution (0.5 g/l) at 25 °C for different time intervals. The amount of MB adsorbed at a time t, q_t, was calculated as:

$$q_t = (C_0 - C_t)\frac{V}{\mathrm{m}} \tag{1}$$

where C_0 is the initial concentration of the dye in the solution, C_t is the dye concentration at a time t, V is the volume of the dye solution and m is the carbon sample weight.

The equilibrium isotherms of adsorption of MB were obtained by soaking 10 mg of the carbon samples in 10 ml of MB solutions of different initial concentrations at 25 °C for 48 h to ensure that the equilibrium was reached. The amount of MB adsorbed at the equilibrium, q_e, was calculated as follows:

$$q_e = (C_0 - C_e)\frac{V}{\mathrm{m}} \tag{2}$$

where C_e is the dye concentration at the equilibrium. The MB concentrations were determined using a UV/Vis spectrophotometer (Heλios-α from Thermo Spectronic) at a wavelength of the maximum of light absorption (665 nm).

3 Results and discussion

3.1 Ordered mesoporous carbons from creosote as the carbon precursor

The SBA-15 template used here exhibited a very well developed mesoporosity with a d_{DFT} = 8.5 nm and S_{BET} = 615 m^2/g (see Figure SI 3 in Supporting Information). The initial attempts of infiltrating the SBA-15 directly with the creosote gave rise to a composite material SBA-15/creosote with *ca.* 30 wt.% of the carbon precursor within the pores of the OMS. However, no carbon material could be retained after the carbonization step. To overcome this issue, we used a catalyst to promote the polymerization of the creosote components by electrophilic aromatic substitution. Specifically, the mixing of the SBA-15 with the creosote was carried out in acidic medium by adding H_2SO_4 to the creosote in a 90 : 10 creosote : H_2SO_4 volumetric ratio (X_S) in a two-step process: first the template was mixed with the creosote and then the H_2SO_4 was added. In this case, the amount of carbon precursor infiltrated in the template (X_{CP}) was 50.1 wt.%. The carbon content in the carbon/SBA-15 composites (X_C) after the carbonization was a mere 14.0 wt.%, so the carbonization yield (η_C) was 16.2 wt.%. The carbon material obtained after removing the template exhibited a well-developed mesoporosity, as it can be seen in Figure SI 3 in Supporting Information, but its XRD pattern indicated that such a mesoporosity was not periodically ordered (see Figure SI 4 in Supporting Information).

Importantly, it was observed that after the creosote was mixed with H_2SO_4 and the mixture was left still overnight, two liquid phases with different densities and viscosities were formed. The density of the phases formed at the top and the bottom was ~1.1 g/cm^3 and ~1.4 g/cm^3, respectively. As explained in the following, the creosote components were dissolved in the H_2SO_4, which corresponded to the bottom phase (*i.e.*, the high-density phase). Using only the high-density phase for the infiltration of the template succeeded in attaining well-developed OMCs as it will be demonstrated. Furthermore, with the aim of studying the effect of H_2SO_4, three different X_S ratios were used for the polymerization of the creosote, namely, 95:5, 90:10 and 80:20. As shown in Table 1, the density of the high-density phase (ρ_{HD}) increased as the H_2SO_4 ratio increased (tending to the density of H_2SO_4, 1.84 g/cm^3), so that the X_{CP} obtained in the SBA-15/Carbon precursor composites also increased. These values were slightly higher than the maximum values of the carbon precursor that could be loaded on the template, which were calculated by assuming that all of the pores of the template were filled with the carbon precursor. Even though the amount of the high-density phase infiltrated in the template was quite high, no agglomeration of the carbon precursor was observed in the outer part of the SBA-15 particles, as can be seen from the comparison of the FE-SEM images of the pristine template and the SBA-15/Carbon precursor composite (see Figure 1 a and b).

Table 1. Density of the high-density phase obtained from creosote mixed with H_2SO_4 at different ratios, and the filling ratios after the infiltration and carbonization of the SBA-15.

X_S (vol.:vol.)	ρ_{HD} (g/cm^3)	X_{CP}* (wt.%)	X_C (wt.%)	η_C (wt.%)
95:5	0.9	50.0 (49.8)	25.8	34.8
90:10	1.4	64.0 (62.1)	37.9	34.4
80:20	1.6	70.5 (65.3)	39.1	26.8

* The values in brackets are the maximum amount of carbon precursor that can be loaded in the porosity of the template. μ

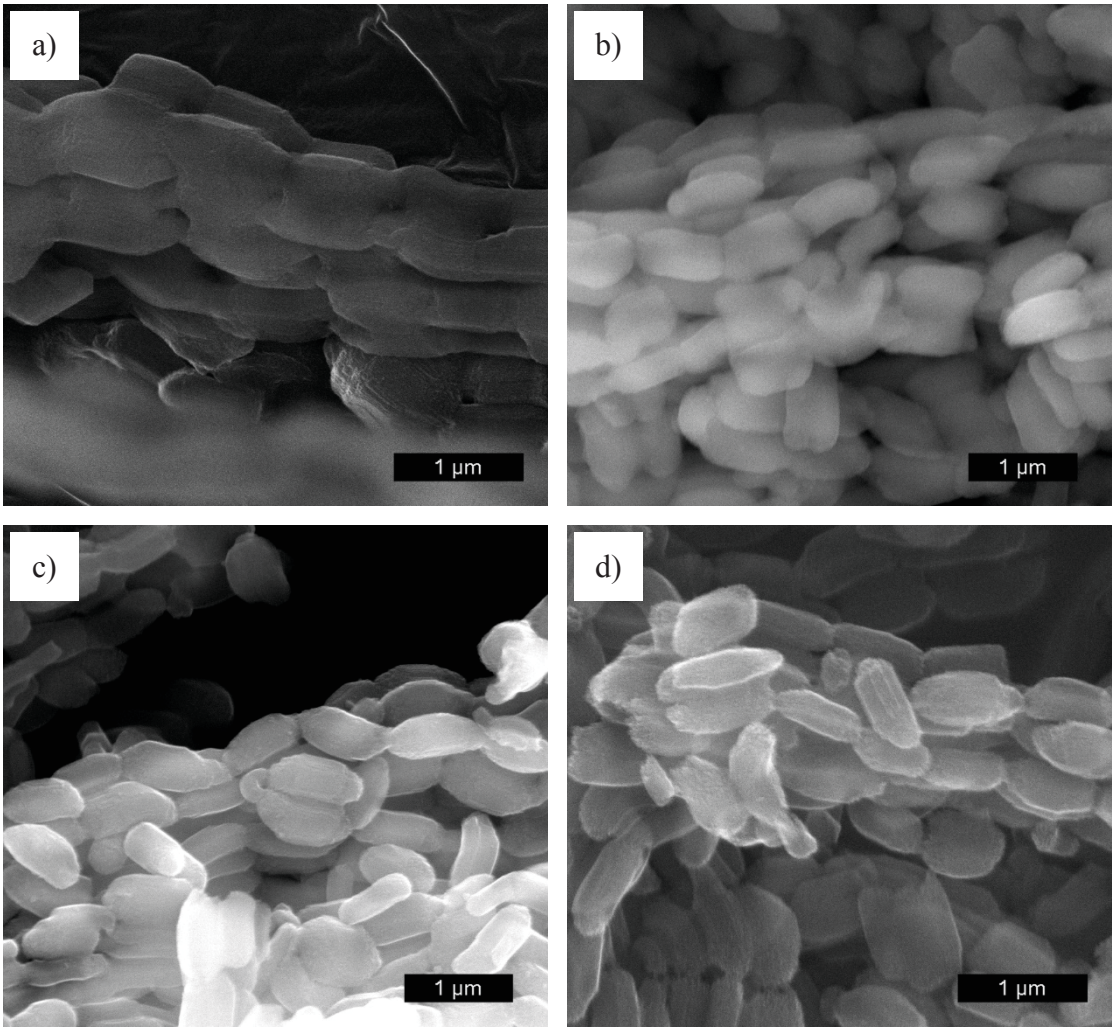

Figure 1. FE-SEM micrographs of the SBA-15 template (a), SBA-15/Carbon precursor (b), SBA-15/Carbon, and OMCreo (X_S=90:10).

The distribution of the creosote components in the presence of H_2SO_4 was further studied. To this end, the two phases formed after the addition of H_2SO_4 in a 90:10 ratio were separated, dissolved in acetone and analyzed by gas chromatography. As shown in Figure 2, the main component in the original creosote was phenanthrene, its content increasing in the high-density phase. In general, aromatic compounds are similarly distributed in both phases, although some differences are observed, probably due to the different solubility of the compounds in H_2SO_4. Interestingly, the high-density phase

became substantially enriched in N-containing compounds (see Figure 2b). This is expected since the N-containing compounds generally possess a basic character and therefore they could have a higher solubility in the acidic H_2SO_4 medium (acid-base interactions). As it was explained in Section 2.1.3, the last step of the infiltration process consisted on heating the SBA-15/creosote mixture at 110 °C under atmospheric pressure for 2 hours. The color of the composite became noticeably darker after this step, suggesting that a certain polymerization of the aromatic compounds catalyzed by H_2SO_4 was taking place. No color change could be noticed for the composite without H_2SO_4. Indeed, this polymerization step was of utmost importance to promote a rise in the carbonization yield, as will be demonstrated below.

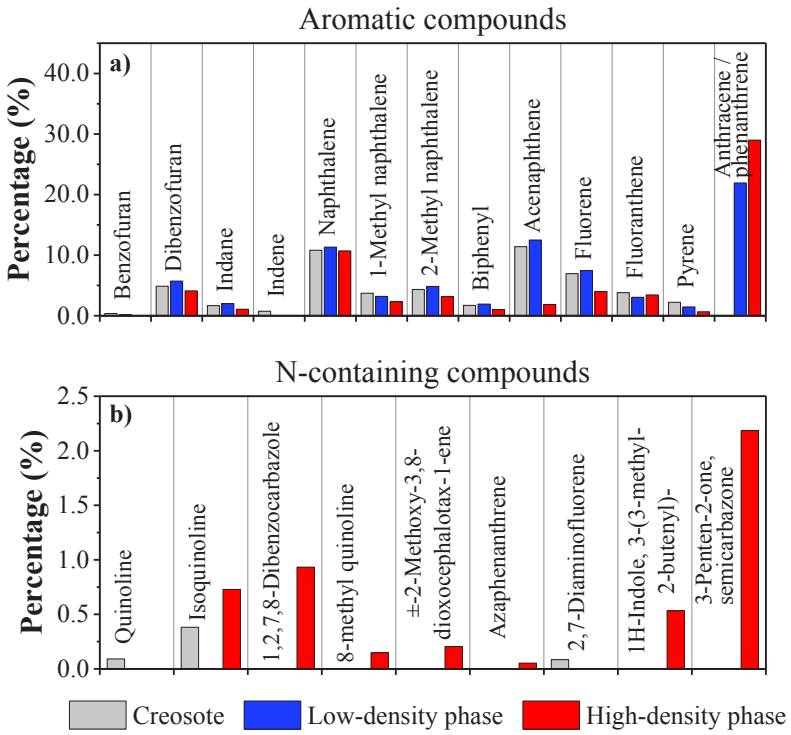

Figure 2. Relative abundance of the components of the creosote and its derivatives obtained in acidic media detected by gas chromatography.

After the SBA-15/carbon precursor composite was submitted to heat treatment, the particles still displayed the same morphology as shown by the FE-SEM images (Figure 1c). The carbon content in the SBA-15/carbon composites (*i.e.*, prior to removing the silica template) as well as the carbonization yield increased as X_S decreased (see Table 1). In the case of X_S=95:5, the amount of carbon that remains in the composite after carbonization was rather low. The N_2 adsorption/desorption isotherm of the SBA-15/carbon composite with X_S=95:5 (see Figure 3) showed that the material was mainly mesoporous, implying that the volume occupied by the carbon in the SBA-15 porosity was rather limited, so only a partial carbon filling of the template was achieved. As for the composite with X_S=80:20, the amount of carbon in the composite was the highest obtained, but the N_2 adsorption/desorption isotherm of the composite revealed that the composite was also somewhat mesoporous, and thus the filling was not complete either. The carbonization yield in this case was the lowest, probably because H_2SO_4 was present in excess. Thus, since the decomposition of H_2SO_4 takes place at temperatures

above 300 °C [28], a significant mass loss should be associated to the removal of this reagent. Nevertheless, the amount of carbon in this sample was rather high.

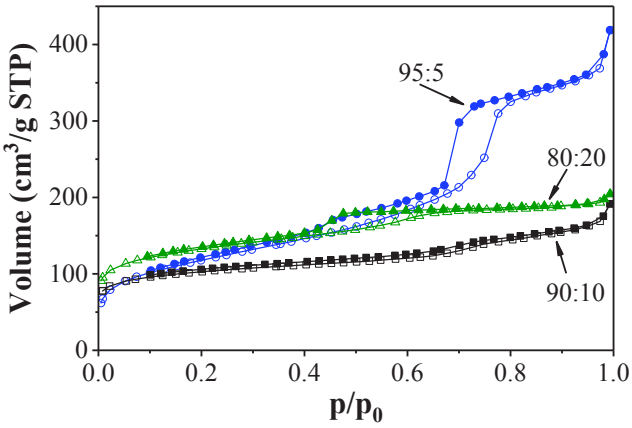

Figure 3. N_2 adsorption isotherms at -196 °C of the SBA-15/carbon composites prepared using the high-density phase obtained from creosote mixed with H_2SO_4 at different ratios.

On the other hand, the X_S ratio of 90:10 gave rise to a carbon precursor with a high carbonization yield (Table 1) and led to a composite material with a high carbon content and the most extensive filling of the OMS mesopores, since the N_2 adsorption/desorption isotherm showed that this material was mainly microporous (Figure 3).

The SBA-15/carbon composites were washed with NaOH to release the carbon material from the template, and the carbon material was named as OMCreo. Figure 4a shows that all the carbon materials obtained with different X_S ratios possessed type IVb N_2 adsorption/desorption isotherms, according to the IUPAC classification, with an H2 hysteresis loop [29] typical of materials with a well-developed mesoporosity but complex porous texture [30]. The N_2 adsorption/desorption isotherm of the OMCreo obtained with X_S=95:5 did not reach a plateau, suggesting that its mesoporosity was relatively heterogeneous, whereas the other two OMCreo samples exhibited a rather homogeneous pore size distribution. The hysteresis loop in the case of the sample prepared with X_S=80:20 was wider than that of the one obtained with X_S=90:10, which indicated that the former sample had a less homogeneous pore size distribution in the mesopore region. Thus, its pore size distribution was wider comparing with that of the sample prepared with X_S=90:10. The micropore volume of the samples increased as the amount of H_2SO_4 increased, and so the specific surface area increased up to 1067 m^2/g (see Table 2).

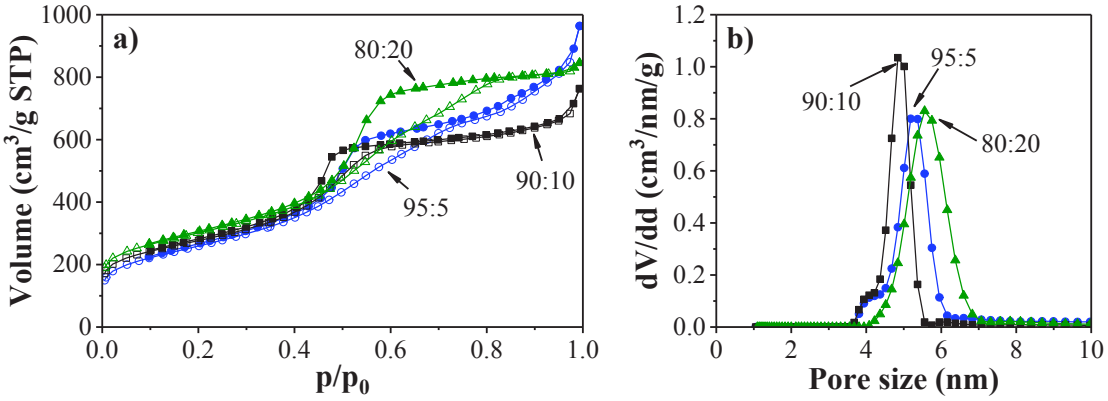

Figure 4. N_2 adsorption isotherms at -196 °C of the OMC prepared using the high-density phase obtained from creosote mixed with H_2SO_4 at different ratios.

Elemental analysis indicated that the sulfur content increased with the amount of H_2SO_4 included in the creosote/H_2SO_4 mixture, but the nitrogen content tended to decrease slightly (Table 2). On the other hand, the carbon content was maximum at X_S=90:10.

Table 2. Textural properties and elemental analysis of the OMC prepared using the high-density phase obtained from creosote mixed with H_2SO_4 at different ratios

X_S (vol.:vol.)	N_2 adsorption				Elemental Analysis			
	S_{BET} (m^2/g)	V_T (cm^3/g)	$V_{\mu p,DR}$ (cm^3/g)	V_{mp} (cm^3/g)	C (wt.%)	H (wt.%)	N (wt.%)	S (wt.%)
95:5	928	1.30	0.34	0.96	83.32	0.61	2.95	0.21
90:10	1017	1.19	0.38	0.81	87.67	0.46	2.81	0.71
80:20	1067	1.27	0.40	0.87	79.66	0.45	2.24	1.79

The XRD pattern of the SBA-15 showed three peaks at 2θ= 0.90°, 1.56° and 1.80°, corresponding to the (1 0 0), (1 1 0) and (2 0 0) reflections (see Figure 5a). The OMCreo sample obtained with X_S=90:10 and X_S=80:20 showed similar XRD patterns to that of the SBA-15 template, which indicated that these OMCreo possessed a well replicated mesostructure. The XRD pattern of the OMCreo obtained with X_S=95:5 still showed a weak (1 0 0) peak at 2θ= 0.95°. In this case, the low carbon filling of the template led to a material with a less ordered and rather heterogeneous pore structure. The unit cell parameter obtained from the interlayer spacing in the (1 0 0) direction (d_{100}) was 11.0 nm for SBA-15 and it decreased to 10.3 nm and 10.0 nm for OMCreo with X_S=90:10 and X_S=80:20, respectively, probably due to a contraction of the template during the carbonization step [12,31]. The wide-angle XRD patterns (see Figure 5b) presented two broad but well-defined peaks at 2θ= 25° and 43°, corresponding to the (0 0 2) and (1 0) reflections. This indicated that the OMCreo materials had a relatively disordered structure similar to that of the OMCs obtained from other aromatic compounds [14], but with a higher graphitization degree than that of the OMCs prepared using pitch or sucrose as carbon precursors [32]. The Raman spectra of the OMCreo materials (see Figure SI 5 in Supporting Information) showed the typical features of disordered carbon materials with almost no difference between the samples. Therefore, the H_2SO_4 ratio had almost no influence in the carbon crystallinity but it had a strong effect on the mesostructure order.

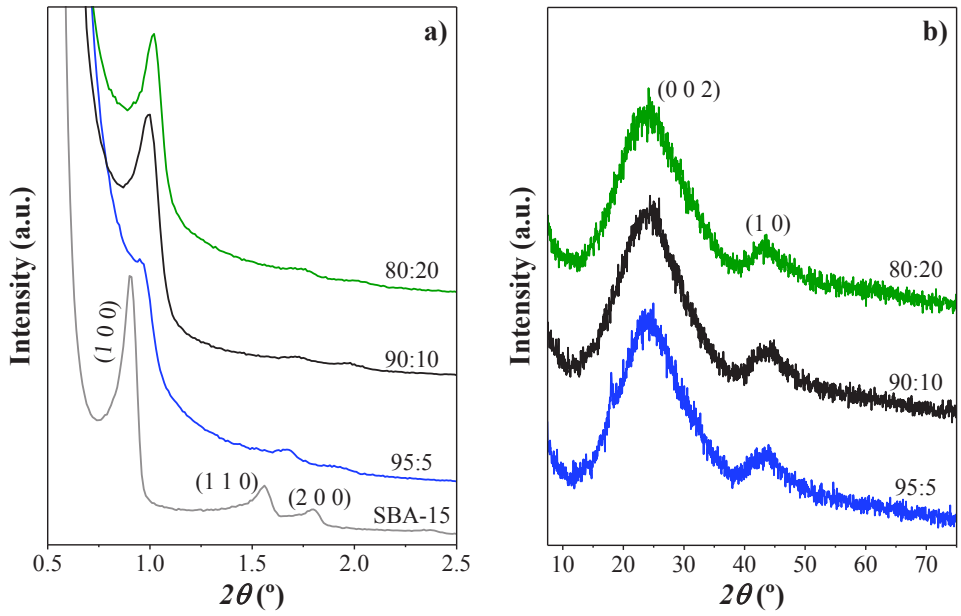

Figure 5. Low-angle (a) and wide-angle (b) XRD patterns of the SBA-15 used as template and the OMC prepared using the high-density phase obtained from creosote mixed with H_2SO_4 at different ratios.

The TEM images of the OMCreo (X_S=90:10) sample (see Figure 6) also demonstrated that the material had a hexagonal array of pores, with a very well ordered mesoporous structure. Moreover, the material was seen to be free of any amorphous carbon material on the outer surface of its constituting particles, as it could have been the case if the carbon precursor was not well infiltrated into the pores of the SBA-15 template.

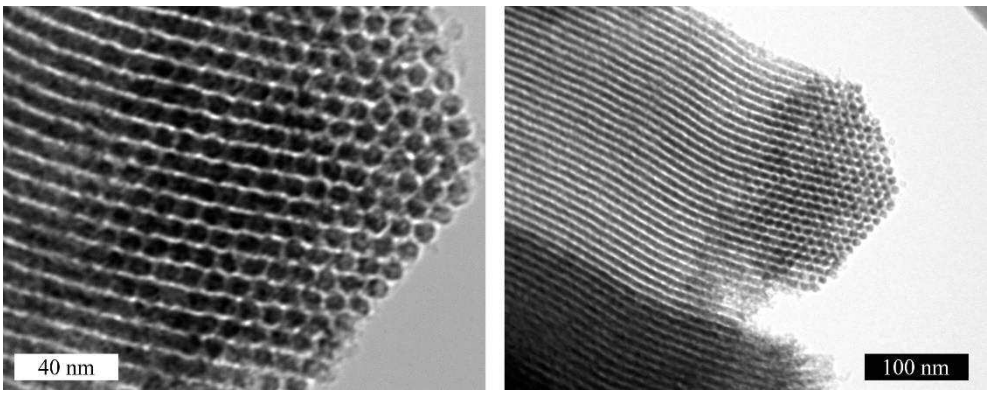

Figure 6. TEM micrographs of OMCreo (X_S=90:10).

Taking into account all these characterization results, a creosote to H_2SO_4 ratio of X_S=90:10 was considered optimal for the preparation of OMC with well-balanced physicochemical properties. Indeed, this material showed a very well ordered mesoporous structure with a very narrow pore size distribution, similar to the ones obtained by impregnation of the same type of template with other carbon precursors such as sucrose [31,32] but narrower than in the case of the ones obtained using chemical vapor deposition [32]. The preparation method of OMCs that is presented here has several advantages over other methods reported in the literature. In the first place, creosote is available in large quantities and at a low price, unlike in the case of single

polycyclic aromatic compounds such as acenaphthene, naphthalene, anthracene, pyrene or phenanthroline that have been used for the preparation of OMCs [12,14–19], and are routinely obtained after the industrial distillation of tars and different purification steps. Furthermore, H_2SO_4 was used in this work, which is much less expensive than the organic acids that have been used in the preparation of OMCs from some of the mentioned polyaromatic compounds. Another advantage is that the preparation was carried out at low pressures, low temperatures and resorting to a one-step impregnation, unlike the case of impregnation with sucrose [31] or furfuryl alcohol [33], where the impregnation step must be repeated several times to obtain good quality OMCs. All of these advantages make the present method more cost-effective and attractive than those previously used with other carbon precursors. The high surface area (1017 m^2/g) and substantial nitrogen content (2.81 wt.%) potentially make this material suitable for use in electrochemical energy storage and pollutant removal, since a hierarchical pore network with nitrogen doping could enhance the performance of porous materials in such applications [34,35].

3.2 Energy and environmental applications

3.2.1 OMCreo as an electrode for supercapacitors

The performance of the materials as electrochemical capacitors was evaluated in 1 M H_2SO_4 electrolyte. A 3-electrode cell was used in the first place to study the behavior of individual electrodes. Figure 7a shows the cyclic voltammograms of the electrodes prepared from OMCreo (X_S=90:10) and the reference activated carbon YP-50F. YP-50F showed two redox peaks at *ca.* 0.3 V *vs.* Ag/AgCl, which is typically associated to the presence of quinone groups on the surface of the carbon materials. Both electrodes exhibited low intrinsic resistance (R_S) attributed to the cell assembly and the ionic resistance of the electrolyte [36], the value of which are obtained from the interception of their corresponding Nyquist plots with the real part of the impedance (Z_{real}) axis at high frequencies (see Figure 7b). R_S was 0.17 and 0.13 Ω/cm^2 for OMCreo and YP-50F respectively. The charge transfer resistance, R_{CT}, comes from the electronic resistance of the electrode and the electrode-electrolyte interface [37]. R_{CT} is given by the diameter of the semicircle observed at medium frequencies in the Nyquist plot (see Figure 7b), and was slightly lower for YP-50F (1.13 Ω/cm^2) than for OMCreo (1.59 Ω/cm^2). However, after the semicircle, at low frequencies, the imaginary part of the impedance (Z_{im}) increased less steeply for YP-50F, probably due to a slow ion diffusion into the porous structure of the YP-50F carbon, while the increase was rather sharp in the case of OMCreo, owing to its ordered porous structure that allows a rapid ion transport [38,39]. The time constant (τ) obtained from the position of the maximum of the plot of the real part of the capacitance *vs.* frequency [40], yielded values of 25.7 s and 8.0 s for YP-50F and OMCreo, respectively. This supports the conclusion of a better diffusion of the ions in the less convoluted pore structure of OMCreo (the porous texture characterization of YP-50F can be found in the Supporting Information).

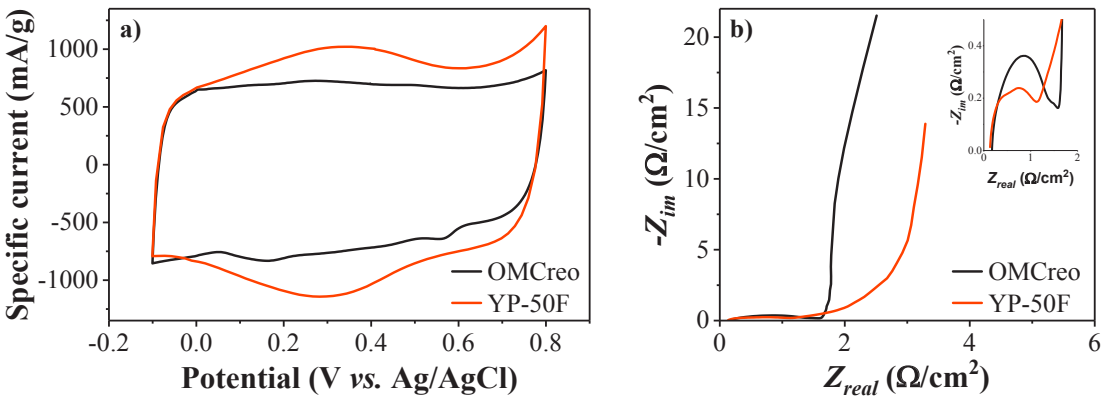

Figure 7. Cyclic voltammograms (sweep rate: 5 mV/s) (a) and Nyquist plots (the impedances were normalized to the electrodes surface) at open circuit voltage of OMCreo and YP-50F measured in 1M H_2SO_4 in a three-electrode cell.

The single electrodes exhibited a higher capacitance for YP-50F (see Table SI 2 in the Supporting Information), which could be mainly attributed to the pseudocapacitance observed in the voltammograms. However, the voltammograms measured in the 2-electrode cells (see Figure SI 7 in Supporting Information) possessed a rectangular shape indicative of almost purely capacitive behavior. The galvanostatic charge/discharge profiles obtained in the 2-electrode cell, shown in Figure 8, are triangularly shaped for both materials, but at high current densities (Figure 8b) the better diffusion of the ions in the OMCreo electrode made the IR drop less significant than in the case of the YP-50F. In this configuration, the capacitance values were similar for both samples, as noticed in Table SI 2 of the Supporting Information, obtaining capacitance values of the whole cells of 38 F/g and 39 F/g for YP-50F and OMCreo, respectively at a current density of 50 mA/g. The capacitance value obtained for OMCreo was very similar to the reported values for mesoporous carbon materials prepared using the hard-template method with SBA-15 as template and sucrose as carbon precursor [41,42] and higher than the capacitance reported for pitch derived OMCs [41]. In general, the OMCreo exhibited capacitance values in agreement with those reported in the literature for OMCs obtained from SBA-15 with similar surface areas (see Figure SI 8 in Supporting Information) [12,41–46].

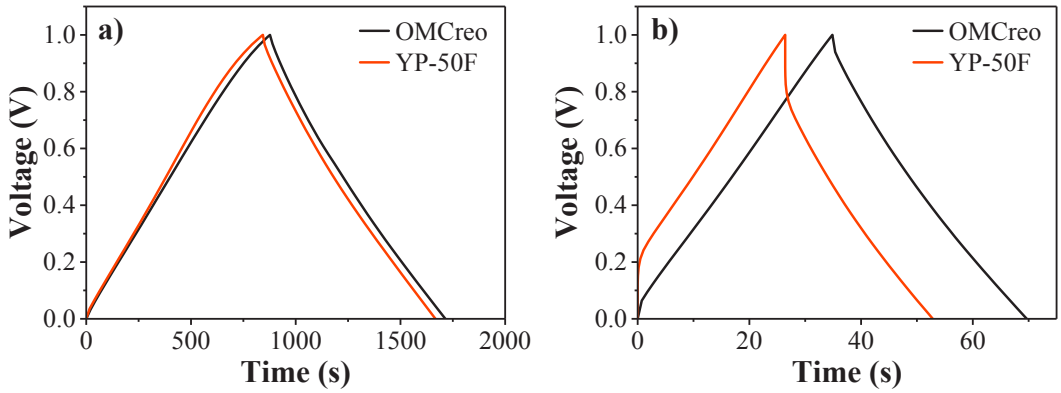

Figure 8. Galvanostatic charge/discharge profiles of the electrodes prepared from OMCreo and YP-50F obtained at a specific current of 50 mA/g (a) and 10 A/g (b) in 1M H_2SO_4 in a two-electrode cell.

The Ragone plots of the capacitors (Figure 9) showed that both samples yielded similar maximum energy densities, but the better performance at high current densities of OMCreo afforded higher power density values (0.43 kW/kg and 2.73 kW/kg for YP-50F and OMCreo, respectively).

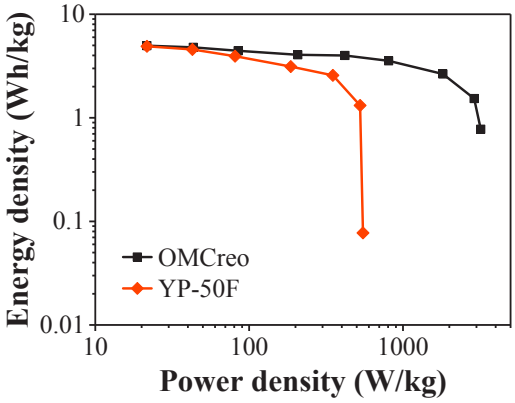

Figure 9. Ragone plot for OMCreo and YP-50F in 1M H_2SO_4.

3.2.2 OMCreo as a dye adsorbent

The OMCreo (X_S=90:10) was also tested as an adsorbent for removing the dye methylene blue (MB) from water. The performance of OMCreo was compared to that of three commercial activated carbons, S300, S1030 and P835, used for a similar purpose. The porous texture characterization of these samples can be found in the Supporting Information. S300 and P835 have type I isotherms (see Figure SI 9), typical of microporous materials, but with some contribution of mesoporosity. S1030 has a higher presence of mesopores, with a wider isotherm knee and hysteresis loop. Thus, these activated carbons are mainly microporous but with different contributions of mesopores, with an increasing mesopore volume in the order P835<S300<S1030 (see Table SI 3).

The equilibrium MB adsorption isotherms (see Figure 10a) were analyzed by the Langmuir model:

$$q_e = \frac{q_m K_L C_e}{1 + K_L C_e} \tag{3}$$

where q_m is the maximum monolayer adsorbed capacity and K_L is the Langmuir constant (see Table 3). It is possible to define a dimensionless equilibrium parameter as:

$$R_L = \frac{1}{1 + K_L C_m} \tag{4}$$

where C_m is the highest dye concentration. R_L indicates whether the shape of the isotherm is favorable ($0<R_L<1$), linear ($R_L=1$) or unfavorable ($R_L>1$) [47]. Even though all of the samples showed a very favorable isotherm shape, with very low R_L values, the lower the micropore volume of the carbon materials, the more favorable the MB adsorption was (see Figure SI 11 in Supporting Information). However, the lower the micropore volume was, the lower the maximum amount adsorbed MB (see Table 3 and Figure SI 10 in Supporting Information). The MB molecular dimensions are 1.40 nm ×

0.60 nm × 0.25 nm, which is in the micropore range, so the MB is likely to be adsorbed in the micropores. The q_{MB} values obtained compared favorably with those of activated carbons [48] and other OMCs [49,50] reported in the literature.

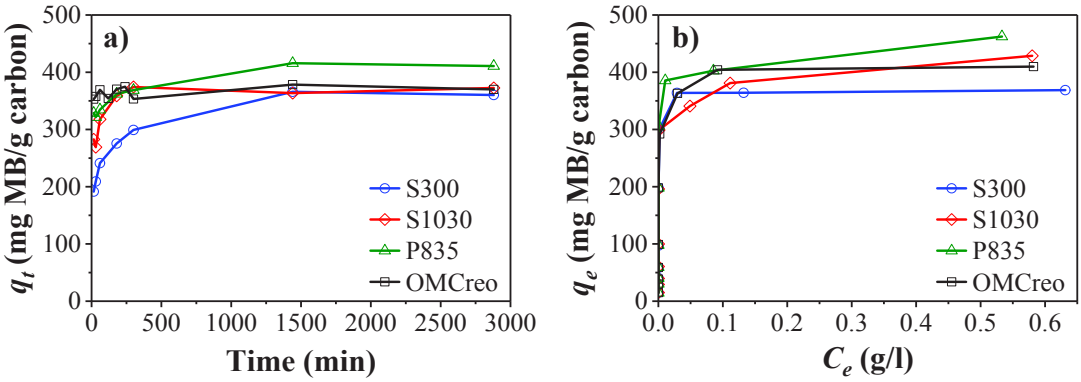

Figure 10. Time-resolved adsorption capacities (a) and equilibrium adsorption isotherms of MB on the commercial activated carbons and OMCreo.

Table 3. Kinetic and equilibrium parameters of the adsorption of MB on the commercial activated carbons and OMCreo.

Sample name	q_{MB} (mg/g)	Second order kinetic model		Langmuir adsorption model		
		q_e (mg/g)	k_2 (×10^{-4} g/mg/min)	q_m (mg/g)	K_L (l/mg)	R_L (×10^{-4})
OMCreo	579.6	369.2	19.864	365.2	5.00	4.99
S300	387.3	313.3	1.779	364.7	5.09	3.92
S1030	570.8	385.0	2.460	342.2	5.05	7.88
P835	569.9	414.7	1.319	395.5	3.72	6.72

The adsorption kinetics data (see Figure 10b) were fitted using the second-order kinetic model (see equation 5) [51] and the results are collected in Table 3:

$$\frac{t}{q_t} = \frac{1}{k_2 q_e^2} + \frac{1}{q_e} t \tag{5}$$

where q_t is the adsorption capacity at a time t, k_2 is the rate constant and q_e is the amount of dye adsorbed in the equilibrium. The k_2 value obtained for OMCreo was very similar to the ones obtained for other OMCs prepared by the hard-template method using SBA-15 as template [49,50] and higher than the ones obtained for activated carbons, carbon nanotubes, graphene or graphene oxide [52–54]. It is possible to establish an almost linear correlation between the rate of adsorption and the mesopore volume of the samples (see Table 3 and Table SI 3 in Supporting Information), as shown in Figure SI 12 in the Supporting Information. Thus, OMCreo showed a very high rate of adsorption thanks to not only its high mesopore volume, but also due to its ordered mesostructure, which would help to drive the adsorbate into the narrow porosity, where its adsorption would be favored.

4 Conclusions

Porous carbons with very well ordered mesoporosity were prepared via the hard-template method using creosote, a low-value coal tar product, as the carbon precursor. The preparation method was optimized via partial polymerization of the creosote in acidic medium, obtaining a material with a high surface area and a very narrow pore size distribution, confined mainly in the range of the mesopores. The well-developed mesoporosity made the material very promising in applications such as electrochemical energy storage and water remediation. Indeed, the material showed very good performance as electrode for supercapacitors and as sorbent of dyes, exceeding the performance of commercial activated carbons used in the same applications. The preparation method can potentially be scaled up, since a rather inexpensive carbon precursor was used, together with a facile template one-step infiltration method at low pressures already used in the industry for the impregnation of wood.

5 Acknowledgment

This project has received funding from the Research Fund for Coal and Steel (RFCS) of the European Union (EU) under grant agreement No 709741. We also acknowledge Bilbaína de Alquitranes S.A. for providing the creosote used in this work, Cabot Corp. for the Vulcan XC72R carbon black, Kuraray Europe GmbH for the FR-20 and YP-50F activated carbons, and Silcarbon GmbH for the S300, S1030 and P835 activated carbons.

6 References

[1] T. Kyotani, Porous carbon, in: E.-I. Yasuda, M. Inagaki, K. Kaneko, M. Endo, A. Oya, Y. Tanabe (Eds.), Carbon Alloy., Elsevier Science, Oxford, 2003: pp. 109–127. doi:10.1016/B978-008044163-4/50007-3.

[2] J. Lee, J. Kim, T. Hyeon, Recent progress in the synthesis of porous carbon materials, Adv. Mater. 18 (2006) 2073–2094. doi:10.1002/adma.200501576.

[3] R. Ryoo, S.H. Joo, M. Kruk, M. Jaroniec, B.R. Ryoo, S.H. Joo, M. Kruk, M. Jaroniec, Ordered mesoporous carbons, Adv. Mater. 13 (2001) 677–681. doi:10.1002/1521-4095(200105)13:9<677::AID-ADMA677>3.0.CO;2-C.

[4] Y. Xia, Z. Yang, R. Mokaya, Templated Porous Carbon Materials: Recent Developments, in: D.W. Bruce, D. O'Hare, R.I. Walton (Eds.), Porous Mater., John Wiley & Sons, Ltd, Chichester, UK, 2011: pp. 217–264. doi:10.1002/9780470711385.ch4.

[5] M. Inagaki, M. Toyoda, Y. Soneda, S. Tsujimura, T. Morishita, Templated mesoporous carbons: Synthesis and applications, Carbon. 107 (2016) 448–473. doi:10.1016/j.carbon.2016.06.003.

[6] H. Zhang, X. He, J. Gu, Y. Xie, H. Shui, X. Zhang, N. Xiao, J. Qiu, Wrinkled porous carbon nanosheets from methylnaphthalene oil for high-performance supercapacitors, Fuel Process. Technol. 175 (2018) 10–16. doi:10.1016/J.FUPROC.2018.03.001.

[7] X. He, X. Li, J. Wang, H. Ma, H. Zhang, Y. Xie, N. Xiao, J. Qiu, From diverse polycyclic aromatic molecules to interconnected graphene nanocapsules for supercapacitors, Microporous Mesoporous Mater. 245 (2017) 73–81. doi:10.1016/J.MICROMESO.2017.02.078.

[8] J. Wang, T.-L. Liu, Q.-X. Huang, Z.-Y. Ma, Y. Chi, J.-H. Yan, Production and characterization of high quality activated carbon from oily sludge, Fuel Process. Technol. 162 (2017) 13–19. doi:10.1016/J.FUPROC.2017.03.017.

[9] S. Gao, B.S. Villacorta, L. Ge, K. Steel, T.E. Rufford, Z. Zhu, Effect of rheological properties of mesophase pitch and coal mixtures on pore development in activated carbon discs with high compressive strength, Fuel Process. Technol. 177 (2018) 219–227. doi:10.1016/J.FUPROC.2018.04.032.

[10] J. Alcañiz-Monge, J.P. Marco-Lozar, M.Á. Lillo-Ródenas, CO_2 separation by carbon molecular sieve monoliths prepared from nitrated coal tar pitch, Fuel Process. Technol. 92 (2011) 915–919. doi:10.1016/J.FUPROC.2010.12.010.

[11] M. Hao, N. Xiao, Y. Wang, H. Li, Y. Zhou, C. Liu, J. Qiu, Pitch-derived N-doped porous carbon nanosheets with expanded interlayer distance as high-performance sodium-ion battery anodes, Fuel Process. Technol. 177 (2018) 328–335. doi:10.1016/J.FUPROC.2018.05.007.

[12] Y. Zhai, Y. Wan, Y. Cheng, Y. Shi, F. Zhang, B. Tu, D. Zhao, The influence of carbon source on the wall structure of ordered mesoporous carbons, J. Porous Mater. 15 (2008) 601–611. doi:10.1007/s10934-007-9139-x.

[13] A.H. Lu, F. Schüth, Nanocasting: A versatile strategy for creating nanostructured porous materials, Adv. Mater. 18 (2006) 1793–1805. doi:10.1002/adma.200600148.

[14] T.-W. Kim, I.-S. Park, R. Ryoo, A synthetic route to ordered mesoporous carbon materials with graphitic pore walls, Angew. Chemie Int. Ed. 42 (2003) 4375–4379. doi:10.1002/ange.200352224.

[15] K.P. Gierszal, T.-W. Kim, R. Ryoo, M. Jaroniec, Adsorption and structural properties of ordered mesoporous carbons synthesized by using various carbon precursors and ordered siliceous P6mm and Ia3d mesostructures as templates, J. Phys. Chem. B. 109 (2005) 23263–23268. doi:10.1021/jp054562m.

[16] C.H. Kim, D.K. Lee, T.J. Pinnavaia, Graphitic mesostructured carbon prepared from aromatic precursors, Langmuir. 20 (2004) 5157–5159. doi:10.1021/la049602c.

[17] S.H. Joo, H.I. Lee, D.J. You, K. Kwon, J.H. Kim, Y.S. Choi, M. Kang, J.M. Kim, C. Pak, H. Chang, D. Seung, Ordered mesoporous carbons with controlled particle sizes as catalyst supports for direct methanol fuel cell cathodes, Carbon. 46 (2008) 2034–2045. doi:10.1016/j.carbon.2008.08.015.

[18] S.H. Joo, C. Pak, D.J. You, S.A. Lee, H.I. Lee, J.M. Kim, H. Chang, D. Seung, Ordered mesoporous carbons (OMC) as supports of electrocatalysts for direct methanol fuel cells (DMFC): Effect of carbon precursors of OMC on DMFC performances, Electrochim. Acta. 52 (2006) 1618–1626. doi:10.1016/j.electacta.2006.03.092.

[19] C. Bosch-Navarro, E. Coronado, C. Martí-Gastaldo, P. Amorós, Confined growth of carbon nanoforms in one-dimension by fusion of anthracene rings inside the pores of MCM-41, Nanoscale. 6 (2014) 7981–90. doi:10.1039/c3nr06669j.

[20] X. Li, K. Wan, Q. Liu, J. Piao, Y. Zheng, Z. Liang, Nitrogen-doped ordered mesoporous carbon: Effect of carbon precursor on oxygen reduction reactions, Chinese J. Catal. 37 (2016) 1562–1567. doi:10.1016/S1872-2067(16)62498-1.

[21] V. Perazzolo, C. Durante, R. Pilot, A. Paduano, J. Zheng, G.A. Rizzi, A. Martucci, G. Granozzi, A. Gennaro, Nitrogen and sulfur doped mesoporous carbon as metal-free electrocatalysts for the in situ production of hydrogen peroxide, Carbon. 95 (2015) 949–963. doi:10.1016/j.carbon.2015.09.002.

[22] D. Zhao, J. Feng, Q. Huo, N. Melosh, G.H. Fredrickson, B.F. Chmelka, G.D. Stucky, Triblock copolymer syntheses of mesoporous silica with periodic 50 to 300 angstrom pores, Science. 279 (1998) 548–552. doi:10.1126/science.279.5350.548.

[23] P. Pařil, Thesis: Wood impregnation, Mendel University in Brno. Faculty of Forestry and Wood Technology, Brno, Chequia, 2016.

[24] M.H. Freeman, T.F. Shupe, R.P. Vlosky, H.M. Barnes, Past, present, and future of the wood preservation industry, Forest Prod. J. 53 (2003) 8–15.

[25] C. Melber, J. Kielhorn, I. Mangelsdorf, IPCS Concise International Chemical Assessment Document 62: Coal tar creosote, 2004.

[26] S.J. Gregg, K.S.W. Sing, Adsorption, Surface Area and Porosity, Academic Press, London; New York, 1982.

[27] A. V. Neimark, Y. Lin, P.I. Ravikovitch, M. Thommes, Quenched solid density functional theory and pore size analysis of micro-mesoporous carbons, Carbon. 47 (2009) 1617–1628. doi:10.1016/J.CARBON.2009.01.050.

[28] D. Schwartz, R. Gadiou, J.-F. Brilhac, G. Prado, G. Martinez, A kinetic study of the decomposition of spent sulfuric acids at high temperature, Ind. Eng. Chem. Res. 39 (2000) 2183–2189. doi:10.1021/IE990801E.

[29] F. Rouquerol, J. Rouquerol, K.S.W. Sing, Adsorption by powders and porous solids, Academic

Press, London, 1999.

[30] M. Thommes, Physical adsorption characterization of nanoporous materials, Chemie Ing. Tech. 82 (2010) 1059–1073. doi:10.1002/cite.201000064.

[31] S. Jun, S.H. Joo, R. Ryoo, M. Kruk, M. Jaroniec, Z. Liu, O. Tetsu, O. Terasaki, Synthesis of new, nanoporous carbon with hexagonally ordered mesostructure, J. Am. Chem. Soc. 122 (2000) 10712–10713. doi:10.1021/JA002261E.

[32] J. Parmentier, S. Saadhallah, M. Reda, P. Gibot, M. Roux, L. Vidal, C. Vix-Guterl, J. Patarin, New carbons with controlled nanoporosity obtained by nanocasting using a SBA-15 mesoporous silica host matrix and different preparation routes, J. Phys. Chem. Solids. 65 (2004) 139–146. doi:10.1016/j.jpcs.2003.10.008.

[33] T.N. Phan, M.K. Gong, R. Thangavel, Y.S. Lee, C.H. Ko, Enhanced electrochemical performance for EDLC using ordered mesoporous carbons (CMK-3 and CMK-8): Role of mesopores and mesopore structures, J. Alloys Compd. 780 (2019) 90–97. doi:10.1016/J.JALLCOM.2018.11.348.

[34] C. Young, T. Park, J.W. Yi, J. Kim, M.S.A. Hossain, Y.V. Kaneti, Y. Yamauchi, Advanced functional carbons and their hybrid nanoarchitectures towards supercapacitor applications, ChemSusChem. 11 (2018) 3546–3558. doi:10.1002/cssc.201801525.

[35] S. Gao, L. Ge, B.S. Villacorta, T.E. Rufford, Z. Zhu, Carbon monoliths by assembling carbon spheres for gas adsorption, Ind. Eng. Chem. Res. 58 (2019) 4957–4969. doi:10.1021/acs.iecr.8b04891.

[36] J. Zhang, X.S. Zhao, On the configuration of supercapacitors for maximizing electrochemical performance, ChemSusChem. 5 (2012) 818–841. doi:10.1002/cssc.201100571.

[37] C. Lei, F. Markoulidis, Z. Ashitaka, C. Lekakou, Reduction of porous carbon/Al contact resistance for an electric double-layer capacitor (EDLC), Electrochim. Acta. 92 (2013) 183–187. doi:10.1016/J.ELECTACTA.2012.12.092.

[38] B.-A. Mei, O. Munteshari, J. Lau, B. Dunn, L. Pilon, Physical interpretations of Nyquist plots for EDLC electrodes and devices, J. Phys. Chem. C. 122 (2018) 194–206. doi:10.1021/acs.jpcc.7b10582.

[39] M. Enterría, A. Castro-Muñiz, F. Suárez-García, A. Martínez-Alonso, J.M.D. Tascón, T. Kyotani, Effects of the mesostructural order on the electrochemical performance of hierarchical micro–mesoporous carbons, J. Mater. Chem. A. 2 (2014) 12023–12030. doi:10.1039/C4TA00778F.

[40] P.L. Taberna, P. Simon, J.F. Fauvarque, Electrochemical characteristics and impedance spectroscopy studies of carbon-carbon supercapacitors, J. Electrochem. Soc. 150 (2003) A292. doi:10.1149/1.1543948 .

[41] C. Vix-Guterl, E. Frackowiak, K. Jurewicz, M. Friebe, J. Parmentier, F. Béguin, Electrochemical energy storage in ordered porous carbon materials, Carbon. 43 (2005) 1293–1302. doi:10.1016/J.CARBON.2004.12.028.

[42] Z. Zhang, G. Wang, Y. Li, X. Zhang, N. Qiao, J. Wang, J. Zhou, Z. Liu, Z. Hao, A new type of ordered mesoporous carbon/polyaniline composites prepared by a two-step nanocasting method for high performance supercapacitor applications, J. Mater. Chem. A. 2 (2014) 16715–16722. doi:10.1039/c4ta03351e.

[43] Y. Yan, Q. Cheng, G. Wang, C. Li, Growth of polyaniline nanowhiskers on mesoporous carbon for supercapacitor application, J. Power Sources. 196 (2011) 7835–7840. doi:10.1016/J.JPOWSOUR.2011.03.088.

[44] J.W. Lang, X. Bin Yan, W.W. Liu, R.T. Wang, Q.J. Xue, Influence of nitric acid modification of ordered mesoporous carbon materials on their capacitive performances in different aqueous electrolytes, J. Power Sources. 204 (2012) 220–229. doi:10.1016/j.jpowsour.2011.12.044.

[45] M. Enterría, A. Castro-Muñiz, F. Suárez-García, A. Martínez-Alonso, J.M.D. Tascón, T. Kyotani, Effects of the mesostructural order on the electrochemical performance of hierarchical micro-mesoporous carbons, J. Mater. Chem. A. 2 (2014). doi:10.1039/c4ta00778f.

[46] Á. Sánchez-Sánchez, T.A. Centeno, F. Suárez-García, A. Martínez-Alonso, J.M.D. Tascón, The importance of electrode characterization to assess the supercapacitor performance of ordered mesoporous carbons, Microporous Mesoporous Mater. 235 (2016) 1–8. doi:10.1016/J.MICROMESO.2016.07.052.

[47] W. Weber, R.K. Chakravorti, Pore and solid diffusion models for fixed bed adsorbers, Am. Inst. Chem. Eng. J. 20 (1974) 229–238.

[48] M. Rafatullah, O. Sulaiman, R. Hashim, A. Ahmad, Adsorption of methylene blue on low-cost adsorbents: A review, J. Hazard. Mater. 177 (2010) 70–80. doi:10.1016/J.JHAZMAT.2009.12.047.

[49] X. Yuan, S.-P. Zhuo, W. Xing, H.-Y. Cui, X.-D. Dai, X.-M. Liu, Z.-F. Yan, Aqueous dye adsorption on ordered mesoporous carbons, J. Colloid Interface Sci. 310 (2007) 83–89. doi:10.1016/J.JCIS.2007.01.069.

[50] X. Peng, D. Huang, T. Odoom-Wubah, D. Fu, J. Huang, Q. Qin, Adsorption of anionic and cationic dyes on ferromagnetic ordered mesoporous carbon from aqueous solution: Equilibrium, thermodynamic and kinetics, J. Colloid Interface Sci. 430 (2014) 272–282. doi:10.1016/J.JCIS.2014.05.035.

[51] Y.S. Ho, J.C.Y. Ng, G. McKay, Kinetics of pollutant sorption by biosorbents: Review, Sep. Purif. Methods. 29 (2000) 189–232. doi:10.1081/SPM-100100009.

[52] Y. Li, Q. Du, T. Liu, X. Peng, J. Wang, J. Sun, Y. Wang, S. Wu, Z. Wang, Y. Xia, L. Xia, Comparative study of methylene blue dye adsorption onto activated carbon, graphene oxide, and carbon nanotubes, Chem. Eng. Res. Des. 91 (2013) 361–368. doi:10.1016/J.CHERD.2012.07.007.

[53] T. Liu, Y. Li, Q. Du, J. Sun, Y. Jiao, G. Yang, Z. Wang, Y. Xia, W. Zhang, K. Wang, H. Zhu, D. Wu, Adsorption of methylene blue from aqueous solution by graphene, Colloids Surfaces B Biointerfaces. 90 (2012) 197–203. doi:10.1016/J.COLSURFB.2011.10.019.

[54] Y. Yao, F. Xu, M. Chen, Z. Xu, Z. Zhu, Adsorption behavior of methylene blue on carbon nanotubes, Bioresour. Technol. 101 (2010) 3040–3046. doi:10.1016/J.BIORTECH.2009.12.042.

Supporting Information

Ordered mesoporous carbons obtained from low–value coal tar products for electrochemical energy storage and water remediation

Alberto Castro-Muñiz[1]*, Sara Lorenzo-Fierro[1], Amelia Martínez-Alonso[1], Juan M.D. Tascón[1], Vanessa Fierro[2], Fabián Suárez-García[1], Juan I. Paredes[1].

[1] Instituto Nacional del Carbón (INCAR-CSIC), C/Francisco Pintado Fe 26, 33011, Oviedo, Spain.
[2] Institute Jean Lamour, UMR CNRS, University of Lorraine, ENSTIB, 27 Rue Philippe Séguin, BP 21042, 88051.

* Corresponding Author: alberto@incar.csic.es

Hard template method

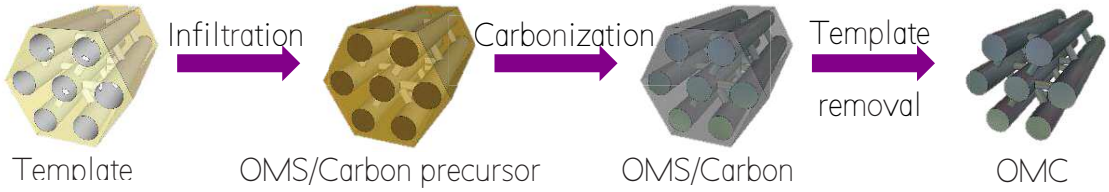

Figure SI 1. Schematic of the preparation of ordered mesoporous carbons via hard template method.

Chromatography

Table SI 1. Qualitative and quantitative (wt.%) chemical composition of the major components present in the coal tar–derived liquid determined by gas chromatography.

Component (wt.%)	Creosote	Low density phase	High density phase
Benzofuran	0.365	0.178	—
Dibenzofuran	4.873	5.723	4.114
Indane	1.662	2.006	1.081
Indene	0.741	—	—
Naphthalene	10.811	11.327	10.712
1–Methyl naphthalene	3.712	3.193	2.315
2–Methyl naphthalene	4.344	4.838	3.147
Biphenyl	1.717	1.927	1.029
Acenaphthene	11.409	12.511	1.855
Fluorene	6.952	7.442	3.992
Fluoranthene	3.814	3.040	3.439
Pyrene	2.223	1.459	0.665
Anthracene or Phenanthrene	20.314	21.937	29.000
Quinoline	0.091	—	—
Isoquinoline	0.382	—	0.729
1,2,7,8–Dibenzocarbazole	—	—	0.933
8–methyl quinoline	—	—	0.148
±–2–Methoxy–3,8–dioxocephalotax–1–ene	—	—	0.205
Azaphenanthrene	—	—	0.053
2,7–Diaminofluorene	0.085	—	—
1H–Indole, 3–(3–methyl–2–butenyl)–	—	—	0.532
3–Penten–2–one, semicarbazone	—	—	2.185
Dibenzotiophene	1.541	—	1.489
Naphtho[2,1–b]thiophene	—	1.735	—
1–Methyldibenzothiophene	0.283	0.231	—
2–Benzothiophene	—	0.577	—
Methylbenzo[b]thiophene	0.051	—	—

Infiltration of the template

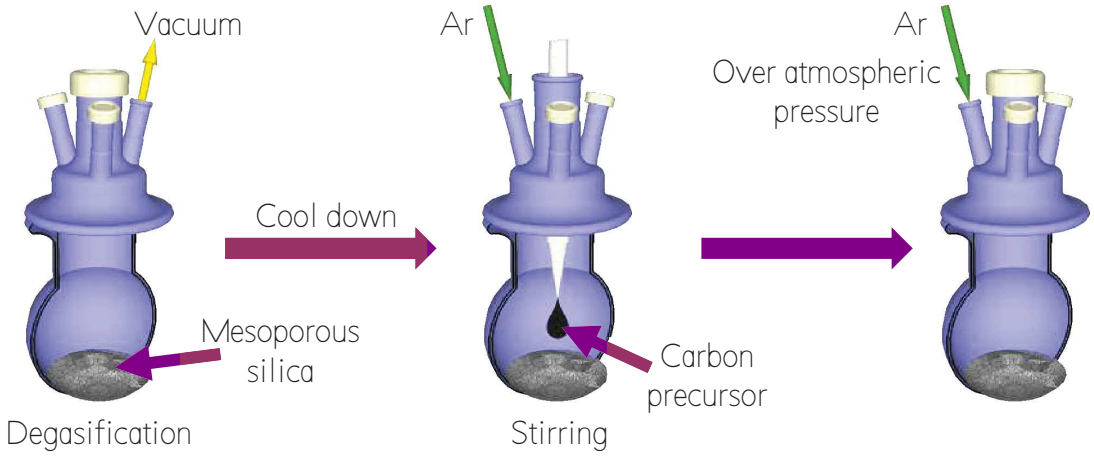

Figure SI 2. Schematic of the infiltration of the mesoporous silica.

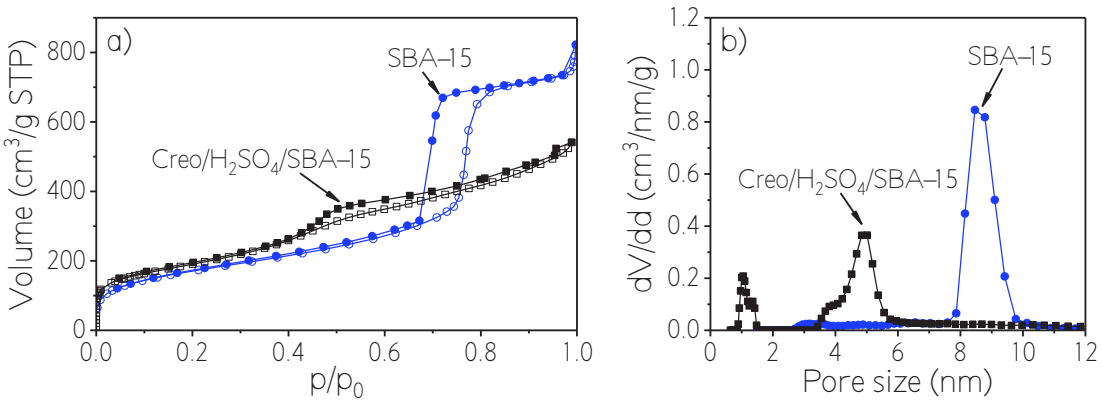

Figure SI 3. N_2 adsorption/desorption isotherms at –196 °C (a) of the SBA–15 template and the carbon obtained using creosote B as carbon precursor in acidic medium (Creo/H_2SO_4/SBA–15) and their corresponding DFT pore size distributions (b).

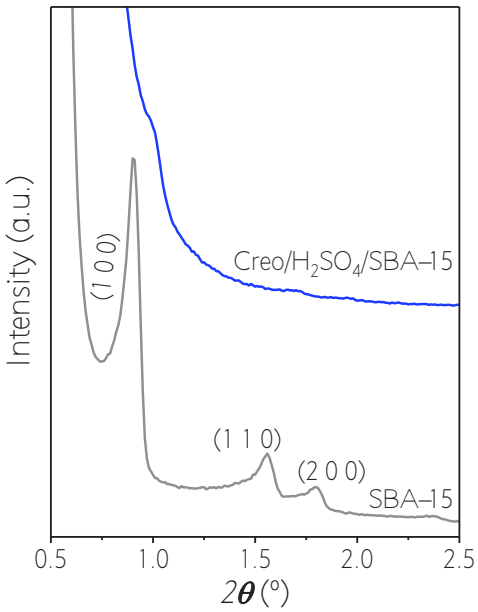

Figure SI 4. Low-angle XRD pattern of the SBA–15 used as template and the carbon material obtained using creosote B as carbon precursor in acidic medium.

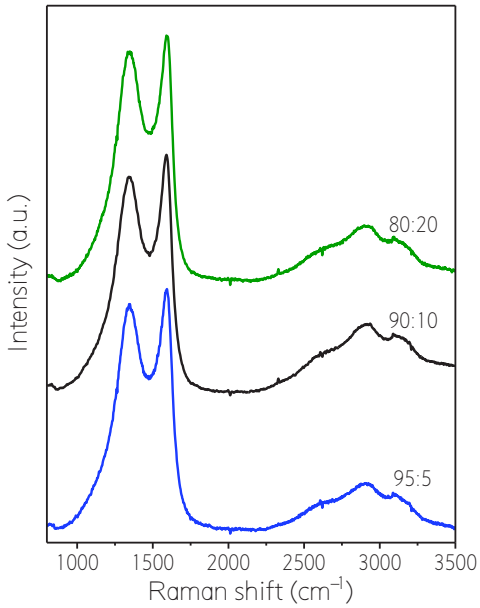

Figure SI 5. Raman spectra of the OMC prepared using the high-density phase obtained from creosote mixed with H_2SO_4 at different ratios.

Electrochemical performance

The specific capacitance values were obtained from the results obtained with different methods as follows:

Cyclic voltammetry

The capacitance can be obtained from the cyclic voltammperograms as C_{CV}:

where is the current intensity as a function of the voltage, ; is the charge and and are the voltage limits; is the sweep rate; and is the mass. In the case of the 3–electrode cell configuration, is the mass of the working electrode while in the 2–electrode cell configuration it was the sum of the mass of both electrodes. In this work, the specific values are given referred to the mass of the active materials in the electrodes.

Galvanostatic charge/discharge

The energy density, *E*, can be calculated from the charge/discharge cycles as:

In this technique the current intensity, , is constant. If the system behavior is nearly capacitive, the energy can be calculated from the capacitance, C_{GCD}, as:

The specific power, *P*, can be obtained as:

Electrochemical impedance spectroscopy

The impedance of a capacitor, , can be expressed as:

where is the angular frequency and *f* is the frequency. The real part of the capacitance at the lowest frequency (C_{EIS}) is the same as the capacitance at galvanostatic discharge. The representation of imaginary part of C_{EIS} *vs. f* goes through a maximum. From the

position of the maximum, it is possible to obtain the time constant, $\tau=1/f$, known as the point at which the system behavior goes from resistive to capacitive.

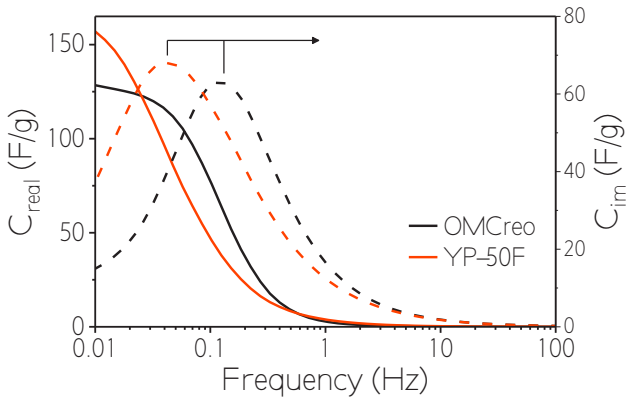

Figure SI 6. Evolution of the real and imaginary capacitance with the frequency at open circuit voltage in 1M H_2SO_4 for the OMCreo and YP–50F.

Table SI 2. Electrochemical performance parameters for the 3–and 2–electrode cells.

Sample	3–electrode cell				2–electrode cell			
	C_{CV}* (F/g)	C_{GCD}** (F/g)	C_{EIS} (F/g)	τ (s)	C_{CV}* (F/g)	C_{GCD}** (F/g)	E** (Wh/kg)	P** (W/kg)
YP–50F	170	178	157	25.7	34	38	4.9	21.7
OMCreo	132	120	128	8.0	38	39	5.0	21.7

* Specific capacitance obtained from cyclic voltammetry at a sweep rate of 5 mV/s.
** Specific capacitance, energy and power obtained from the galvanostatic charge/discharge cycling at 50 mA/g.

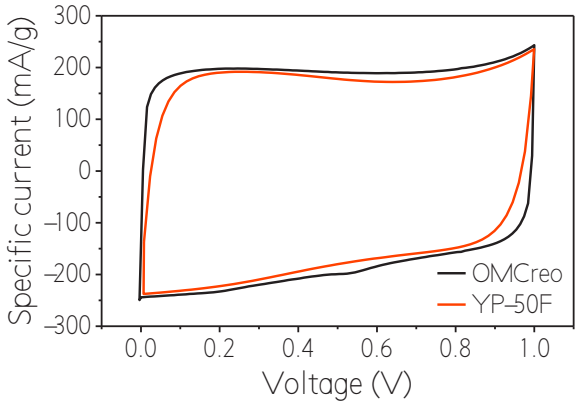

Figure SI 7. Cyclic voltammograms (sweep rate: 5 mV/s) of OMCreo and YP–50F measured in 1M H_2SO_4 in a two–electrode cell.

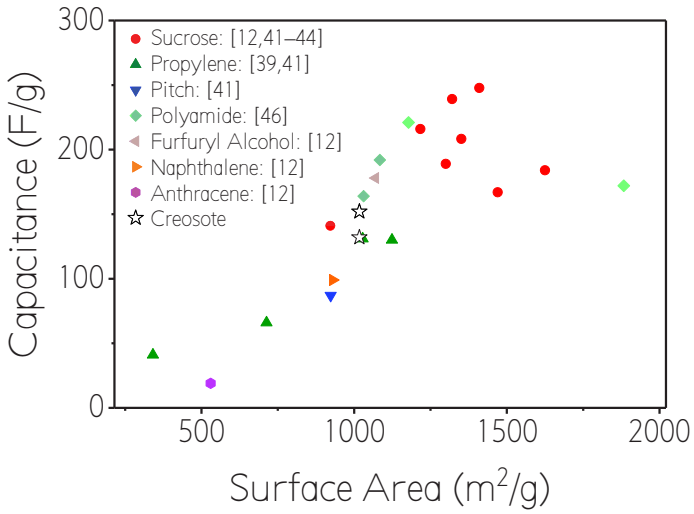

Figure SI 8. Specific capacitance of one electrode measured in H_2SO_4 electrolyte as a function of the surface area for ordered mesoporous carbons using the hard-template method with SBA-15 as template and different carbon precursors reported in the bibliography. The reference numbers are the same as the ones included in the manuscript.

Commercial activated carbons porous texture

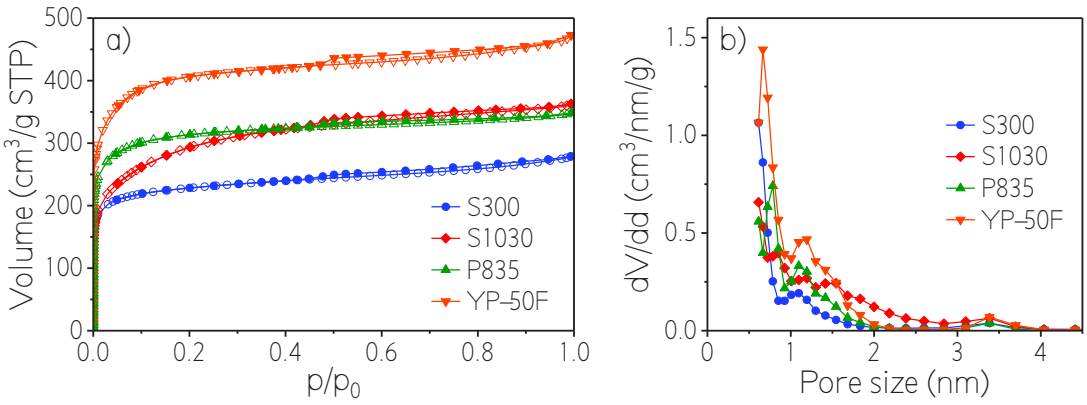

Figure SI 9. N_2 adsorption/desorption isotherms at –196 °C of the commercial activated carbons (a) and their corresponding pore size distributions (b).

Table SI 3. Porous textural parameters derived from N_2 adsorption isotherms at –196 °C of the commercial activated carbon samples.

Sample name	N_2 adsorption			
	S_{BET} (m^2/g)	V_T (cm^3/g)	$V_{\mu p,DR}$ (cm^3/g)	V_{mp} (cm^3/g)
S300	842	0.43	0.33	0.07
S1030	1073	0.55	0.37	0.10
P835	1196	0.53	0.44	0.03
YP–50F	1563	0.72	0.56	0.06

Dye adsorption

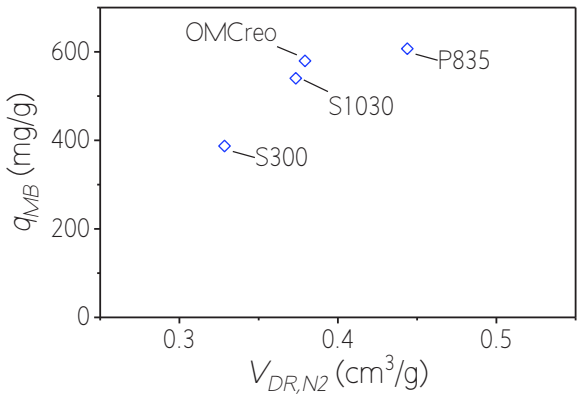

Figure SI 10. Maximum MB adsorption capacity as a function of the micropore volume of the carbon materials.

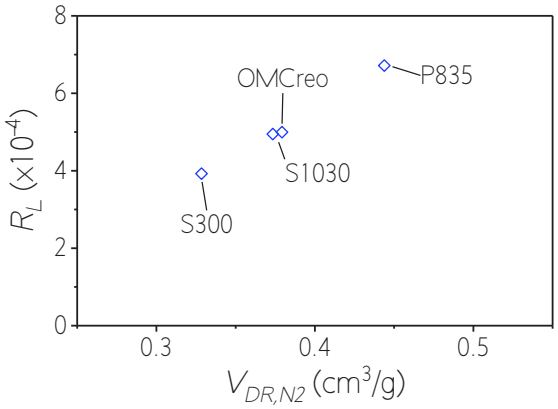

Figure SI 11. Equilibrium parameter as a function of the micropore volume of the carbon materials.

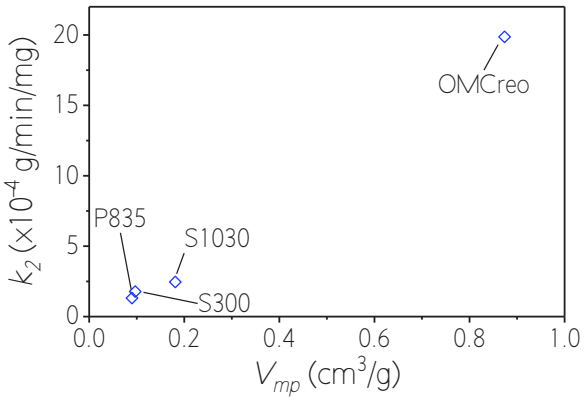

Figure SI 12. Rate constant as a function of mesopore volume of the carbon materials.

Supporting Information

Ordered mesoporous carbons obtained from low-value coal tar products for electrochemical energy storage and water remediation

Alberto Castro-Muñiz[1]*, Sara Lorenzo-Fierro[1], Amelia Martínez-Alonso[1], Juan M.D. Tascón[1], Vanessa Fierro[2], Fabián Suárez-García[1], Juan I. Paredes[1].

[1] Instituto Nacional del Carbón (INCAR-CSIC), C/Francisco Pintado Fe 26, 33011, Oviedo, Spain.
[2] Institute Jean Lamour, UMR CNRS, University of Lorraine, ENSTIB, 27 Rue Philippe Séguin, BP 21042, 88051.

* Corresponding Author: alberto@incar.csic.es

Hard template method

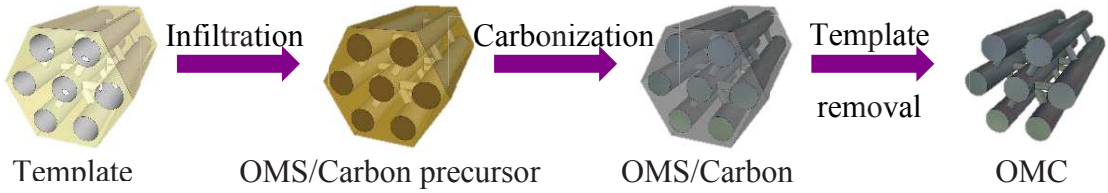

Figure SI 1. Schematic of the preparation of ordered mesoporous carbons via hard template method.

Chromatography

Table SI 1. Qualitative and quantitative (wt.%) chemical composition of the major components present in the coal tar-derived liquid determined by gas chromatography.

Component (wt.%)	Creosote	Low density phase	High density phase
Benzofuran	0.365	0.178	—
Dibenzofuran	4.873	5.723	4.114
Indane	1.662	2.006	1.081
Indene	0.741	—	—
Naphthalene	10.811	11.327	10.712
1-Methyl naphthalene	3.712	3.193	2.315
2-Methyl naphthalene	4.344	4.838	3.147
Biphenyl	1.717	1.927	1.029
Acenaphthene	11.409	12.511	1.855
Fluorene	6.952	7.442	3.992
Fluoranthene	3.814	3.040	3.439
Pyrene	2.223	1.459	0.665
Anthracene or Phenanthrene	20.314	21.937	29.000
Quinoline	0.091	—	—
Isoquinoline	0.382	—	0.729
1,2,7,8-Dibenzocarbazole	—	—	0.933
8-methyl quinoline	—	—	0.148
±-2-Methoxy-3,8-dioxocephalotax-1-ene	—	—	0.205
Azaphenanthrene	—	—	0.053
2,7-Diaminofluorene	0.085	—	—
1H-Indole, 3-(3-methyl-2-butenyl)-	—	—	0.532
3-Penten-2-one, semicarbazone	—	—	2.185
Dibenzotiophene	1.541	—	1.489
Naphtho[2,1-b]thiophene	—	1.735	—
1-Methyldibenzothiophene	0.283	0.231	—
2-Benzothiophene	—	0.577	—
Methylbenzo[b]thiophene	0.051	—	—

Infiltration of the template

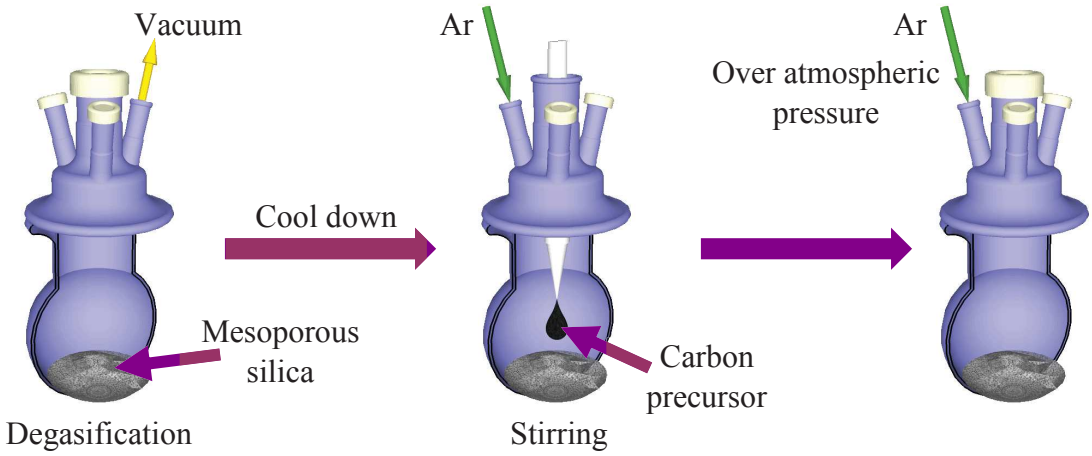

Figure SI 2. Schematic of the infiltration of the mesoporous silica.

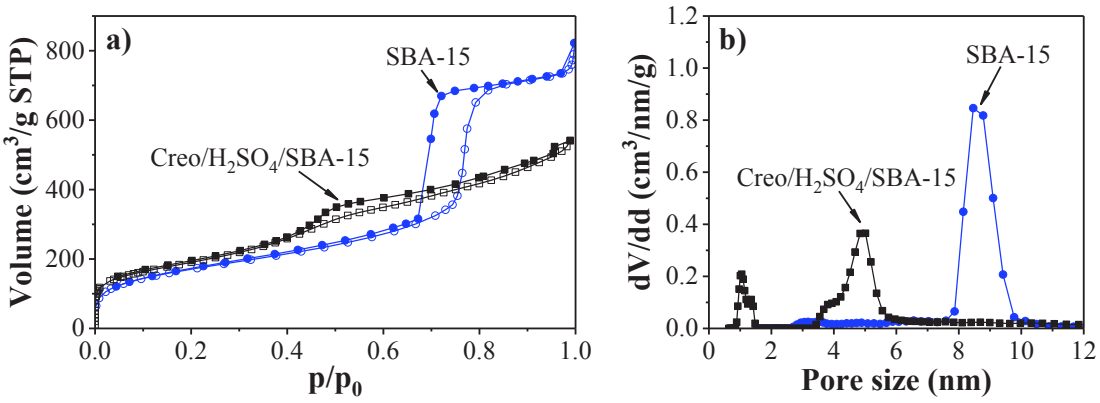

Figure SI 3. N_2 adsorption/desorption isotherms at -196 °C (a) of the SBA-15 template and the carbon obtained using creosote B as carbon precursor in acidic medium (Creo/H_2SO_4/SBA-15) and their corresponding DFT pore size distributions (b).

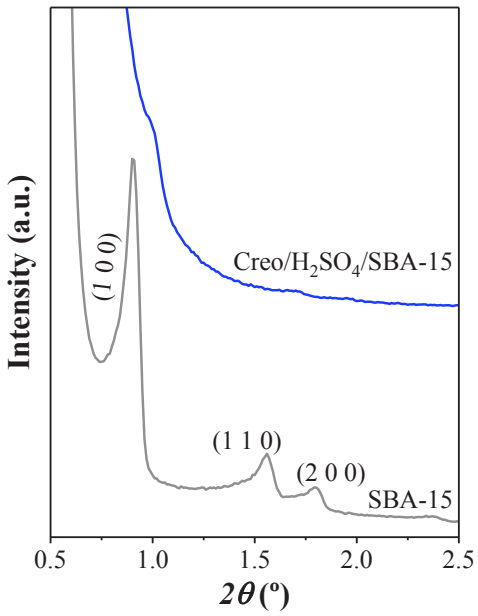

Figure SI 4. Low-angle XRD pattern of the SBA-15 used as template and the carbon material obtained using creosote B as carbon precursor in acidic medium.

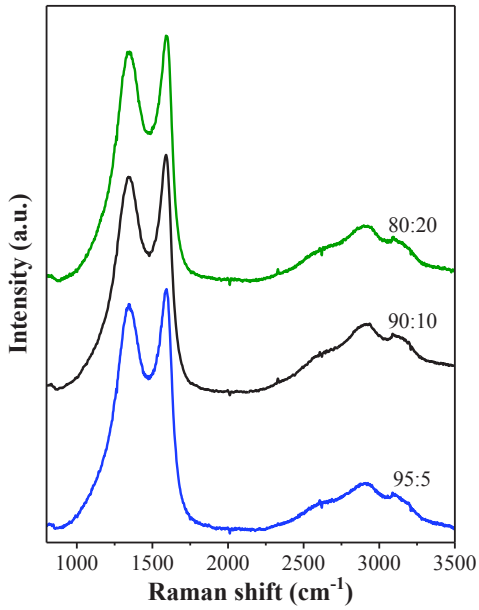

Figure SI 5. Raman spectra of the OMC prepared using the high-density phase obtained from creosote mixed with H_2SO_4 at different ratios.

Electrochemical performance

The specific capacitance values were obtained from the results obtained with different methods as follows:

Cyclic voltammetry

The capacitance can be obtained from the cyclic voltammperograms as C_{CV}:

$$C_{CV} = \frac{1}{m}\frac{Q}{V} = \frac{1}{m}\frac{\int_{t_1}^{t_2} i(t)dt}{V_2 - V_1} = \frac{1}{m}\frac{1}{2\,(V_2 - V_1)\,S_r}\int_{V_1}^{V_2} i(V)dV$$

where $i(V)$ is the current intensity as a function of the voltage, V; Q is the charge and V_1 and V_2 are the voltage limits; S_r is the sweep rate; and m is the mass. In the case of the 3-electrode cell configuration, m is the mass of the working electrode while in the 2-electrode cell configuration it was the sum of the mass of both electrodes. In this work, the specific values are given referred to the mass of the active materials in the electrodes.

Galvanostatic charge/discharge

The energy density, *E*, can be calculated from the charge/discharge cycles as:

$$E = \frac{1}{m}\int_0^Q V dQ = \frac{1}{m}\int_0^t V(t)i(t)dt = \frac{1}{m} i \int_0^t V(t)dt$$

In this technique the current intensity, i, is constant. If the system behavior is nearly capacitive, the energy can be calculated from the capacitance, C_{GCD}, as:

$$E = \frac{1}{2} C_{GCD}(V_2 - V_1)^2 \Rightarrow C_{GCD} = \frac{2E}{(V_2 - V_1)^2}$$

The specific power, *P*, can be obtained as:

$$P = \frac{E}{t}$$

Electrochemical impedance spectroscopy

The impedance of a capacitor, Z, can be expressed as:

$$Z = Z_{real} + jZ_{im} = -\frac{j}{\omega C};\; C = C_{real} - jC_{im}$$

$$C_{real}(\omega) = -\frac{Z_{im}}{\omega|Z|^2} = -\frac{Z_{im}}{2\pi f|Z|^2}$$

$$C_{im}(\omega) = \frac{Z_r}{\omega|Z|^2} = \frac{Z_r}{2\pi f|Z|^2}$$

where ω is the angular frequency and *f* is the frequency. The real part of the capacitance at the lowest frequency (C_{EIS}) is the same as the capacitance at galvanostatic discharge. The representation of imaginary part of C_{EIS} *vs.* *f* goes through a maximum. From the

position of the maximum, it is possible to obtain the time constant, $\tau=1/f$, known as the point at which the system behavior goes from resistive to capacitive.

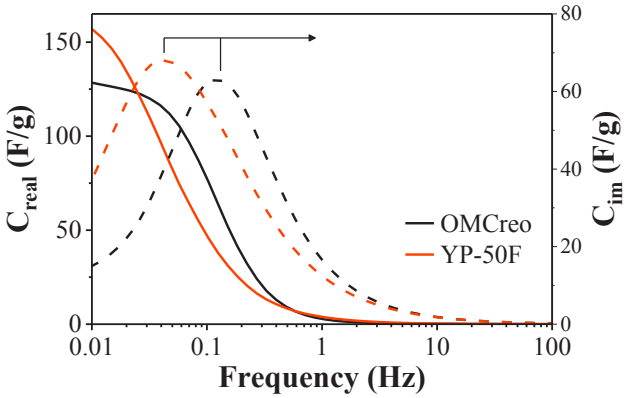

Figure SI 6. Evolution of the real and imaginary capacitance with the frequency at open circuit voltage in 1M H_2SO_4 for the OMCreo and YP-50F.

Table SI 2. Electrochemical performance parameters for the 3- and 2-electrode cells.

Sample	3-electrode cell				2-electrode cell			
	C_{CV}* (F/g)	C_{GCD}** (F/g)	C_{EIS} (F/g)	τ (s)	C_{CV}* (F/g)	C_{GCD}** (F/g)	E** (Wh/kg)	P** (W/kg)
YP-50F	170	178	157	25.7	34	38	4.9	21.7
OMCreo	132	120	128	8.0	38	39	5.0	21.7

* Specific capacitance obtained from cyclic voltammetry at a sweep rate of 5 mV/s.
** Specific capacitance, energy and power obtained from the galvanostatic charge/discharge cycling at 50 mA/g.

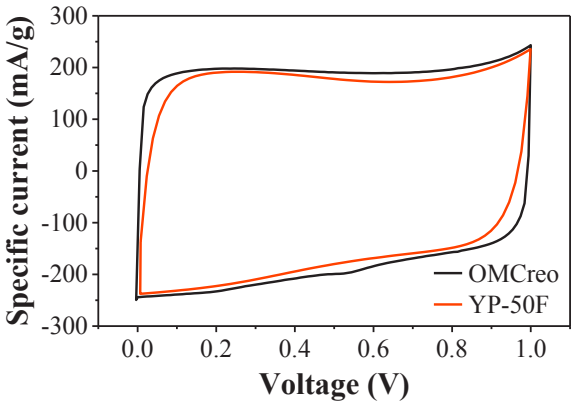

Figure SI 7. Cyclic voltammograms (sweep rate: 5 mV/s) of OMCreo and YP-50F measured in 1M H_2SO_4 in a two-electrode cell.

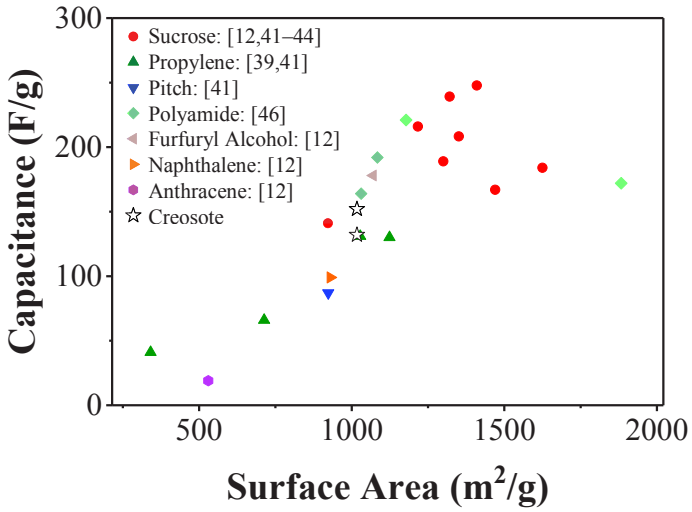

Figure SI 8. Specific capacitance of one electrode measured in H_2SO_4 electrolyte as a function of the surface area for ordered mesoporous carbons using the hard-template method with SBA-15 as template and different carbon precursors reported in the bibliography. The reference numbers are the same as the ones included in the manuscript.

Commercial activated carbons porous texture

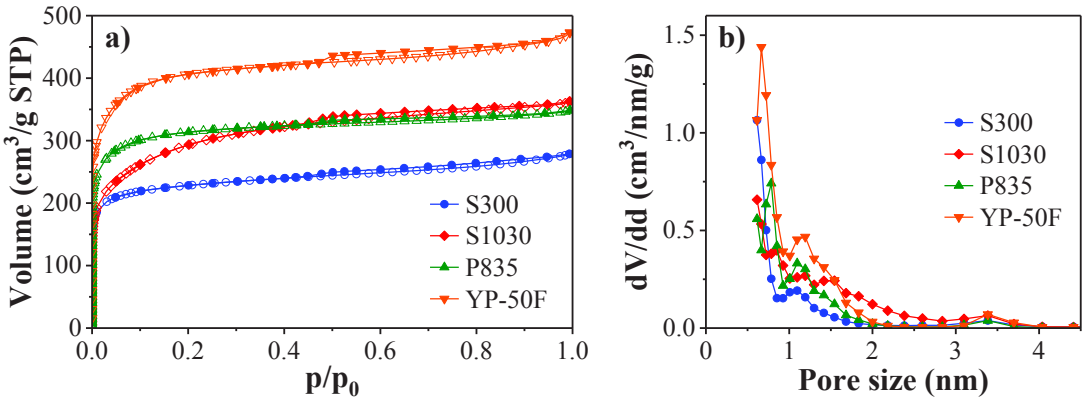

Figure SI 9. N_2 adsorption/desorption isotherms at -196 °C of the commercial activated carbons (a) and their corresponding pore size distributions (b).

Table SI 3. Porous textural parameters derived from N_2 adsorption isotherms at -196 °C of the commercial activated carbon samples.

Sample name	N_2 adsorption			
	S_{BET} (m^2/g)	V_T (cm^3/g)	$V_{\mu p,DR}$ (cm^3/g)	V_{mp} (cm^3/g)
S300	842	0.43	0.33	0.07
S1030	1073	0.55	0.37	0.10
P835	1196	0.53	0.44	0.03
YP-50F	1563	0.72	0.56	0.06

Dye adsorption

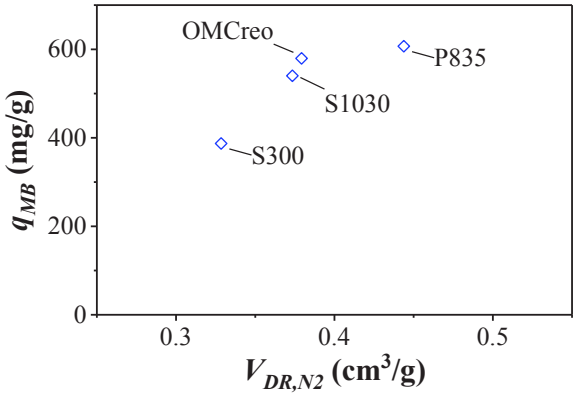

Figure SI 10. Maximum MB adsorption capacity as a function of the micropore volume of the carbon materials.

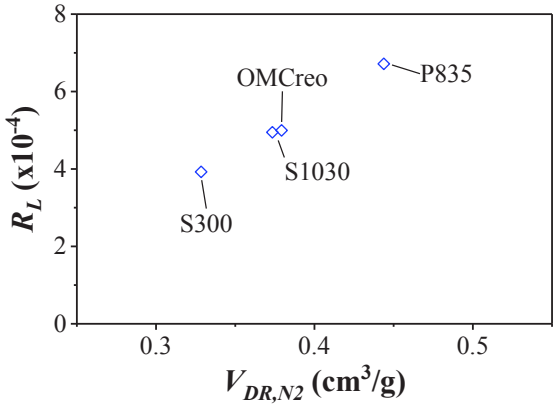

Figure SI 11. Equilibrium parameter as a function of the micropore volume of the carbon materials.

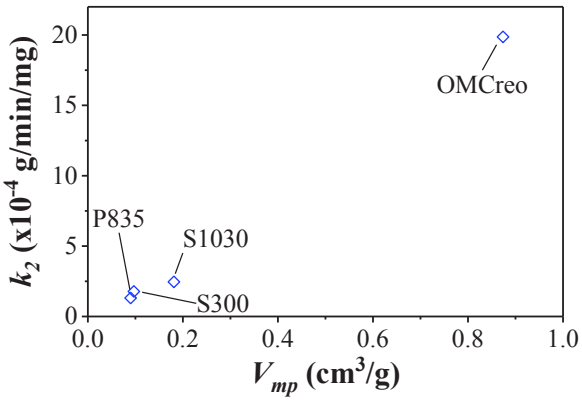

Figure SI 12. Rate constant as a function of mesopore volume of the carbon materials.